minerals

MDPI

Article

Petrogenesis of the Early Paleoproterozoic Felsic Metavolcanic Rocks from the Liaodong Peninsula, NE China: Implications for the Tectonic Evolution of the Jiao-Liao-Ji Belt, North China Craton

Changquan Cheng [1], Jin Liu [2,*], Jian Zhang [1,3], Hongxiang Zhang [2], Ying Chen [1], Xiao Wang [1], Zhongshui Li [2] and Hongchao Yu [2]

[1] School of Earth Sciences and Engineering, Sun Yat-sen University, Guangzhou 510275, China
[2] College of Earth Sciences, Jilin University, Changchun 130061, China
[3] Department of Earth Sciences, The University of Hong Kong, Pokfulam Road, Hong Kong, China
* Correspondence: liujin@jlu.edu.cn

Abstract: The early Paleoproterozoic (ca. 2.2–2.1 Ga) tectonic evolution of the Jiao–Liao–Ji belt (JLJB) is a continuous hot topic and remains highly controversial. Two main tectonic regimes have been proposed for the JLJB, namely arc-related setting and intra-continental rift. Abundant ca. 2.2–2.1 Ga volcanic rocks were formed in the JLJB, especially in the Liaodong Peninsula. These ca. 2.2–2.1 Ga volcanic rocks therefore could host critical information for the evolution of the JLJB. In this study, we report a suit of ca. 2.2–2.1 Ga felsic metavolcanic rocks in the Liaodong Peninsula of the JLJB to provide new insights into the above issue. Zircon U-Pb dating reveals that the felsic metavolcanic rocks were erupted at 2185–2167 Ma. They have variable εHf(t) values (−0.70 to +9.69), high SiO_2 (66.30–75.30 wt.%) and relatively low TiO_2 (0.03–0.78 wt.%), tFe_2O_3 (0.55–5.03 wt.%), MgO (0.17–8.76 wt.%), Cr (9.16–67.30 ppm), Co (2.01–7.00 ppm) and Ni (3.90–25.70 ppm) contents with enrichments in light rare earth element (REE) and large ion lithophile element (LILE), and depletions in heavy REE and high field strength element (HFSE). Geochemical and isotopic results indicate that the felsic metavolcanic rocks were sourced from partial melting of ancient Archean TTG rocks and juvenile lower crustal materials. Combined with coeval A-type granites, bimodal volcanic rocks and the absence of typical arc magmatism, the most likely tectonic regime at ca. 2.2–2.1 Ga for the JLJB is an intra-continental rift.

Keywords: felsic metavolcanic rocks; geochemistry; intra-continental rift; Jiao-Liao-Ji Belt; North China Craton

Citation: Cheng, C.; Liu, J.; Zhang, J.; Zhang, H.; Chen, Y.; Wang, X.; Li, Z.; Yu, H. Petrogenesis of the Early Paleoproterozoic Felsic Metavolcanic Rocks from the Liaodong Peninsula, NE China: Implications for the Tectonic Evolution of the Jiao-Liao-Ji Belt, North China Craton. *Minerals* **2023**, *13*, 1168. https://doi.org/10.3390/min13091168

Academic Editor: Jaroslav Dostal

Received: 13 August 2023
Revised: 30 August 2023
Accepted: 1 September 2023
Published: 3 September 2023

1. Introduction

The North China Craton (NCC) experienced continuous evolution processes of continental crust formation, subduction, collision and cratonization during the Archean to Paleoproterozoic [1–9]. It can be generally divided into the Western Block (WB), the Eastern Block (EB) and the intervening North-South-trending Trans-North China Orogen (TNCO) [3,10,11] (Figure 1a). The WB can be further subdivided into two microblocks (i.e., Yinshan and Ordos blocks), and they are separated by the Paleoproterozoic East-West-trending Khondalite Belt [1,12]. The EB is formed via the amalgamation of the Longgang and Nangrim blocks along the northeast-southwest-trending Jiao-Liao-Ji Belt (JLJB) during the Paleoproterozoic [3,13–17].

The JLJB underwent polyphase structural deformation, magmatism, metamorphism and sedimentation during the Paleoproterozoic orogenesis [18–24] (Figure 1b). Although numerous geochronological, geochemical, metamorphic, and structural studies have been carried out in the JLJB [13,19,22,24–32], its tectonic evolution during the Paleoproterozoic remains highly controversial [21,22,24,32,33]. Currently, there are three main tectonic models: (1) the first model involves oceanic subduction and arc/continent-continent collision between the Longgang and Nangrim blocks [27,30,34–39]; (2) the second model suggests the opening and closure of an intra-continental rift for the tectonic evolution of the JLJB [13,14,25,40–42]; (3) the third model proposes that the JLJB experienced early intra-continental rift and subsequent oceanic subduction and collision [3,17,21–23]. In recent years, increasingly studies suggest an extension tectonic regime for the JLJB during the early Paleoproterozoic (ca. 2.2–2.1 Ga) [14,21,22,31,32,38,43–46]. However, there is still a key dispute whether such an extension is a consequence of back-arc basin or intra-continental rift [22,24,32,38,43,44,46]. Therefore, the ca. 2.2–2.1 Ga magmatism can serve as a significant object of study to provide crucial constrains for the above dispute.

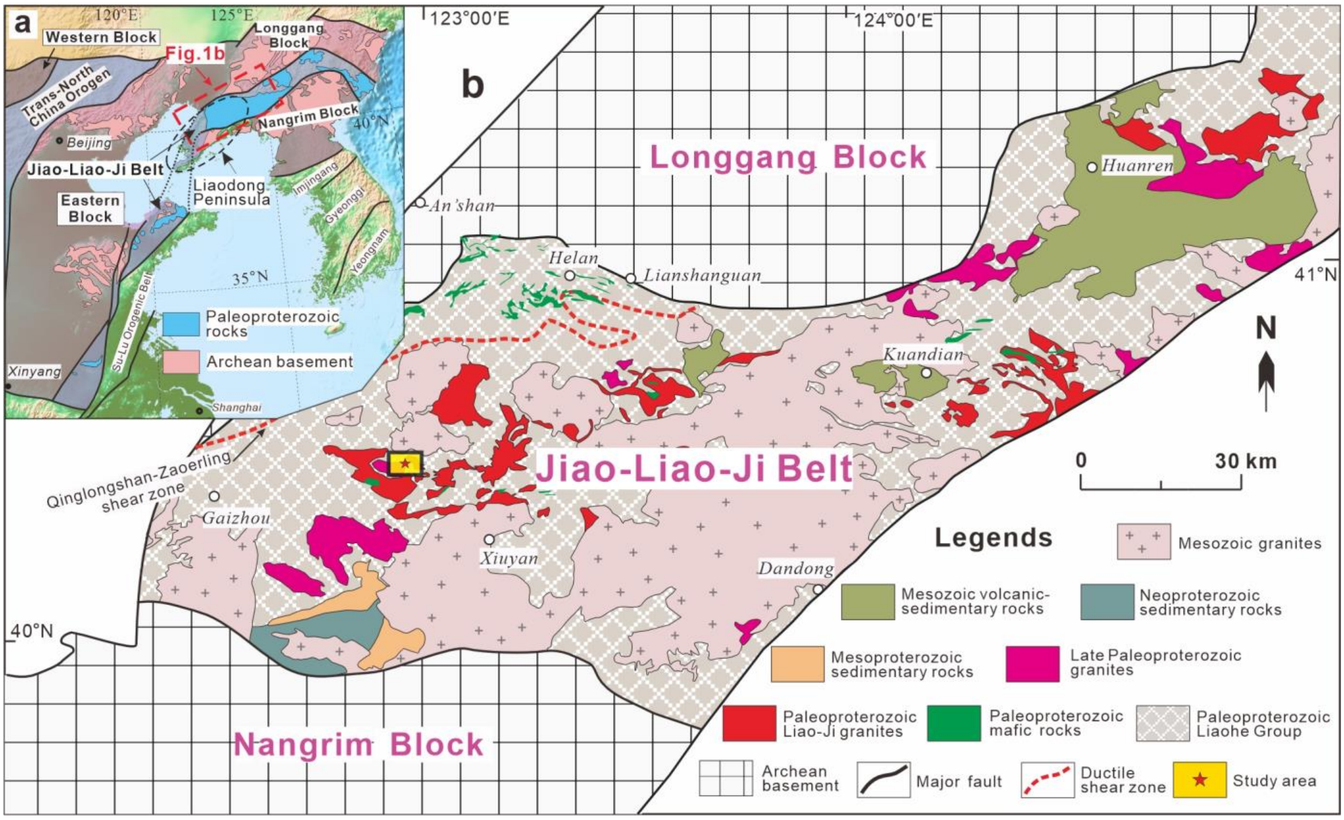

Figure 1. (**a**) Simplified map showing tectonic units of the eastern North China Craton [1,3]; (**b**) Geological map of the Liaodong Peninsula showing main lithological units [13].

Most recently, we implemented detailed geological investigations and identified a suit of felsic metavolcanic rocks in the Houxianyu area (Figure 2), where there is one of the best exposures in the northern Liaodong Peninsula, NE China. In this contribution, new petrology, zircon U-Pb geochronology, bull-rock major and trace elements and zircon Lu-Hf isotopic compositions are reported for the newly identified felsic metavolcanic rocks in the Liaodong Peninsula, with the aim of deciphering their timing of formation, petrogenesis, and tectonic setting, and thus further providing new constrains for the tectonic evolution of the JLJB during the Paleoproterozoic.

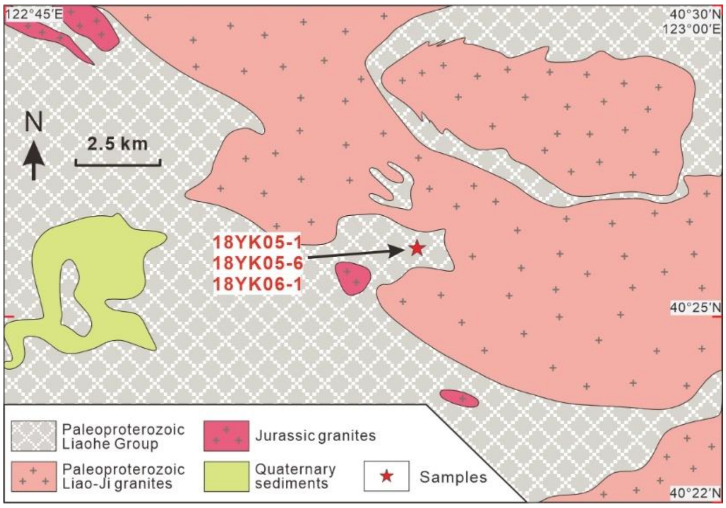

Figure 2. Simplified geological map of the Houxianyu area showing the sampling location.

2. Geological Background

The Paleoproterozoic JLJB is a ca. 1200 km long orogenic belt in the eastern part of the NCC, and geographically it traverses the northern Korean Peninsula, southern Jilin Province, Liaodong and Jiaodong peninsulas, and Anhui Province from northeast to southwest [3,47] (Figure 1a). It is tectonically bounded by the two Archean microblocks (i.e., the Longgang Block to the northwest and the Nangrim Block to the southeastern) [3] (Figure 1a). The Longgang Block mainly consists of abundant Neoarchean tonalite-trondhjemite-granodiorite (TTG) gneisses and supracrustal rocks (e.g., pelitic rock, amphibolite and granulite) and a small volume of Eoarchean to Mesoarchean granitoids [7,48–54]. The Nangrim Block, located in southern Liaoning Province and in North Korea, is composed of Neoarchean granitoid and supracrustal rocks [55–58]. The JLJB mainly consists of Paleoproterozoic granitoids, metamafic intrusions and voluminous metavolcanic-metasedimentary successions with variable metamorphic grades ranging from greenschist to amphibolite facies and locally granulite facies [13,15,18,21–23,25,29,31,32,38,45,59].

As a major terrane of the JLJB, the Liaodong Peninsula is mainly composed of various Paleoproterozoic granitic and mafic intrusive rocks and the Paleoproterozoic Liaohe Group [13,22,23,30,31,44,46,59–61] (Figure 1b). The Paleoproterozoic granitoids are widespread in the Liaodong Peninsula, including ca. 2.20–2.16 Ga Liaoji gneissic granitoids (mainly A-type granites) and ca. 1.90–1.85 Ga post-collision associated granitoids (e.g., undeformed syenite and porphyritic monzogranite) [21–23,28,45,61]. The Paleoproterozoic mafic intrusive rocks are mainly distributed in the northern Liaodong Peninsula (e.g., Helan, Longchang, Jidongyu areas), and a small number of mafic intrusions are also distributed in the Xiuyan and Kuandian areas [31,33,36,38,44,46]. They contain greenschist, plagioclase amphibolite, meta-gabbro and meta-diabase, and have emplacement ages of ca. 2.15–2.10 Ga. The ca. 2.20–2.10 Ga felsic and mafic intrusive rock assemblages were generally deformed and show obvious gneissic structures [21,22,31,38,46]. The Paleoproterozoic Liaohe Group, from bottom to top, can be further subdivided into five units, including the Langzishan, Li'eryu, Gaojiayu, Dashiqiao and Gaixian formations [13,18]. The Liaohe Group is a suit of volcanic-sedimentary rocks and mainly comprises schist, marble, biotite gneiss, fine-grained felsic gneiss, meta-clastic rock, meta-rhyolite and meta-basalt [18]. Traditionally, the Liaohe Group, on the basis of metamorphic and lithological features, is subdivided into the North Liaohe and South Liaohe groups [13].

During the Late Paleoproterozoic, the JLJB underwent widespread and intense high-grade metamorphism [15–17,26,29,62]. More and more mafic and pelitic granulites, characterized by clockwise P-T paths, have been identified in the Liaodong and Jiaodong peninsulas [15–17,20,26,29,62,63]. Such high-grade metamorphism is interpreted as the result of the ca. 1.90 Ga collision event between the Nangrim and Longgang blocks, which marks the final assembly of the EB in the eastern NCC [3]. After the Late Paleoproterozoic orogenic event, the crystalline basement of the eastern NCC was overlain by Meso- to Neoproterozoic sedimentary rocks and experienced intense magmatism and structural deformation during the Mesozoic [64].

3. Petrography

A suit of felsic metavolcanic rocks of this study were newly identified in the Houxianyu area of the northern Liaodong Peninsula (Figure 2). These felsic rocks belong to metamorphosed volcano-sedimentary rock units of the Li'eryu Formation, Liaohe Group. The Paleoproterozoic and Mesozoic granitoids are in tectonic or intrusive contacts with these volcanic sequences. The felsic metavolcanic rocks of this study mainly consist of fine-grained meta-dacite and fine-grained meta-rhyolite, with layered or massive structures (Figure 3). The sample lithologies and locations and the methods applied to each rock sample are summarized in Table 1.

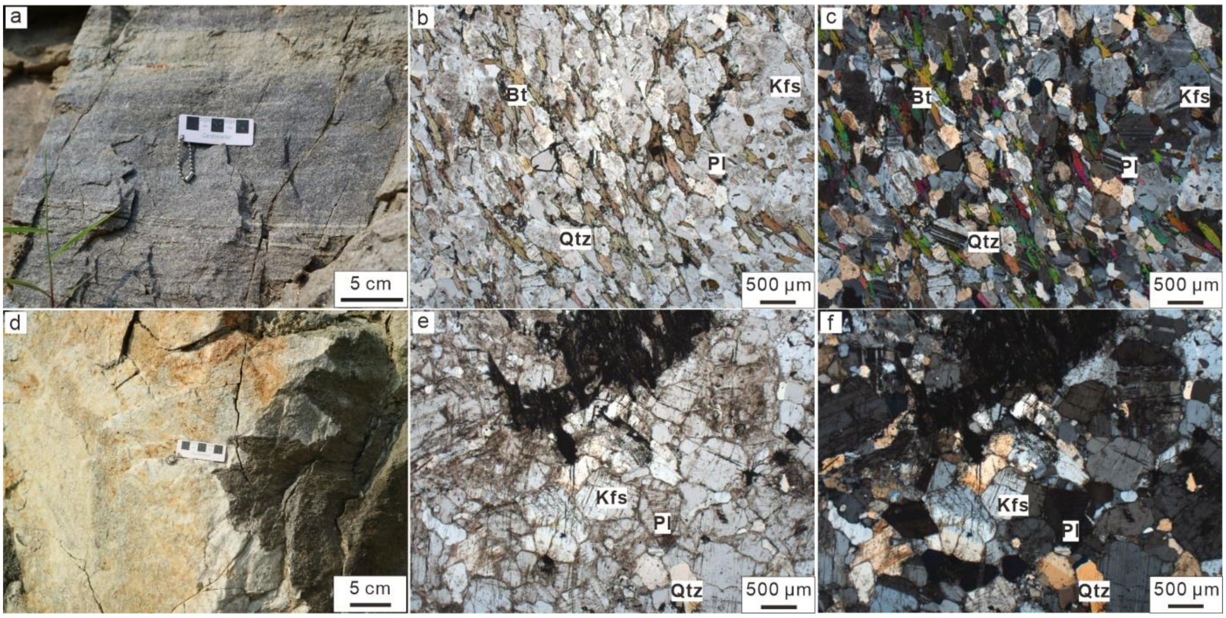

Figure 3. Representative field photographs and microphotographs of the felsic metavolcanic rocks. (**a**–**c**) Fine-grained meta-dacites (Sample 18YK05-9); (**d**–**f**) Fine-grained meta-rhyolites (Sample 18YK05-6). Abbreviations: Pl, plagioclase; Qtz, quartz; Kfs, K-feldspar; Bt, biotite.

Table 1. The simplified list of the felsic metavolcanic rock samples in this study.

Sample	Lithology	GPS	Methods
18YK05-1	Meta-dacite		Zircon U-Pb dating and Lu-Hf isotopic analyses
18YK05-2	Meta-dacite	40°25′56.7″ N; 122°54′32.8″ E	Whole-rock geochemistry
18YK05-3	Meta-dacite		Whole-rock geochemistry
18YK05-6	Meta-rhyolite		Zircon U-Pb dating and Lu-Hf isotopic analyses
18YK05-7	Meta-dacite	40°25′56.5″ N; 122°54′32.5″ E	Whole-rock geochemistry
18YK05-8	Meta-rhyolite		Whole-rock geochemistry
18YK05-9	Meta-dacite		Whole-rock geochemistry
18YK06-1	Meta-rhyolite		Zircon U-Pb dating and Lu-Hf isotopic analyses
18YK06-2	Meta-rhyolite	40°25′57.9″ N; 122°54′34.1″ E	Whole-rock geochemistry
18YK06-4	Meta-dacite		Whole-rock geochemistry

The fine-grained meta-dacites are grey to white in color and occur as deformed layers (Figure 3a). They generally display weakly gneissic structures and fine-grained crystalloblastic textures, with a typical mineral assemblage of plagioclase (~37 vol.%), quartz (~35 vol.%), biotite (~18 vol.%), K-feldspar (~5 vol.%) and minor accessory minerals (~5 vol.%; e.g., tourmaline, zircon, apatite and some opaque minerals) (Figure 3b,c). The majority of these minerals are subhedral to anhedral, with grain sizes of 200–600 µm (Figure 3c).

The fresh surfaces of the fine-grained meta-rhyolites are light in color, and the rocks generally occur as blocks in field outcrops (Figure 3d). They are granular and show fine-grained crystalloblastic textures (Figure 3e). Compared with the fine-grained meta-dacites, the dominant mineral assemblage of the fine-grained meta-rhyolites contains fewer dark-colored minerals, and it is composed of plagioclase (~45 vol.%), quartz (~35 vol.%), K-feldspar (~12 vol.%), and a few other minerals (~8 vol.%; e.g., biotite, tourmaline, zircon and apatite) (Figure 3e,f). Most of these minerals are subhedral to anhedral, with grain sizes ranging from 200 to 1000 µm (Figure 3f).

4. Analytical Methods

4.1. Zircon U-Pb Dating

Three representative felsic metavolcanic rock samples were collected for the zircon U-Th-Pb isotope and trace element analyses (Table 1). Zircon grains were separated from crushed samples using combined techniques of magnetic separation and standard density methods. Typical and clear zircon grains without cracks were handpicked through the binocular microscope, and then fixed on an epoxy disk. After being ground and polished, the zircon grains were imaged by cathodoluminescence (CL) and reflected/transmitted light. Zircon U-Th-Pb isotopic compositions, as well as trace element concentrations, were measured using the instruments of laser ablation (LA) inductively coupled plasma (ICP)-mass spectrometry (MS) at the Yanduzhongshi Geological Analysis Laboratories, Beijing, China. A total of 100 spots on zircon grains were analyzed, with a beam size of 30 µm in diameter. The data acquisition durations for each analysis spot included 20–30 s blank background acquisition and a sample measuring time of 50 s. Standard zircon 91,500 and NIST610 were utilized as external standards for the U-Th-Pb isotopes and trace element compositions of dated zircon grains. Quantitative calibrations for acquired original isotopic and trace element data were carried out using the ICPMSDataCal software [65]. Sample weighted mean or intercept age calculations and Concordia diagrams were performed through the Isoplot program [66].

4.2. Bulk-Rock Geochemistry

A total of seven felsic metavolcanic rock samples were selected for bulk-rock major and trace element analyses (Table 1). Prior to geochemical analysis, fresh rock samples were crushed and powdered to <200 mesh in a completely cleaned agate mill. Bulk-rock major element concentrations were measured using a Leeman Prodigy ICP-optical emission spectroscopy (OES) system at the State Key Laboratory of Geological Processes and Mineral Resources, China University of Geosciences, Beijing, China. Loss on ignition (LOI) values were determined through placing 1 g of bulk-rock powders in the muffle furnace for two hours at a temperature condition of 1000 °C, and then cooling and reweighing residual samples. The acquired results yielded analytical uncertainties better than 2% for most of the major elements. Bulk-rock trace and rare earth element concentration analyses were performed through an Agilent 7500a quadrupole ICP-MS instrument system. The acquired results yielded analytical accuracies generally better than 5% for most of the trace elements.

4.3. Zircon Lu-Hf Isotopic Analyses

The above three felsic metavolcanic rock samples, which had been dated by LA-ICP-MS, were used for in situ zircon Hf isotopic composition analyses at the Yanduzhongshi Geological Analysis Laboratories, Beijing, China. All analyses were conducted using the LA-MC-ICP-MS instrument system (a Neptune multi-collector (MC)-ICP-MS instrument equipped with a NewWave UP213 LA system). A total of 45 representative zircon Lu-Hf test spots were analyzed, similar or close to U-Pb dating domains. The beam size for each spot was ~40 μm in diameter. The test conditions included 16 J/cm^2 laser energy density and an 8 Hz laser repetition rate. More specific and detailed analytical procedures, instrument conditions and experimental processes were described by Wu et al. (2006) [67].

5. Analytical Results

5.1. Zircon U-Pb Geochronology

Zircon U-Pb isotopic data, CL images and Concordia diagrams for three felsic metavolcanic rock samples (18YK05-1, 18YK05-6 and 18YK06-1) are presented in Supplementary Table S1, Figures 4 and 5, respectively.

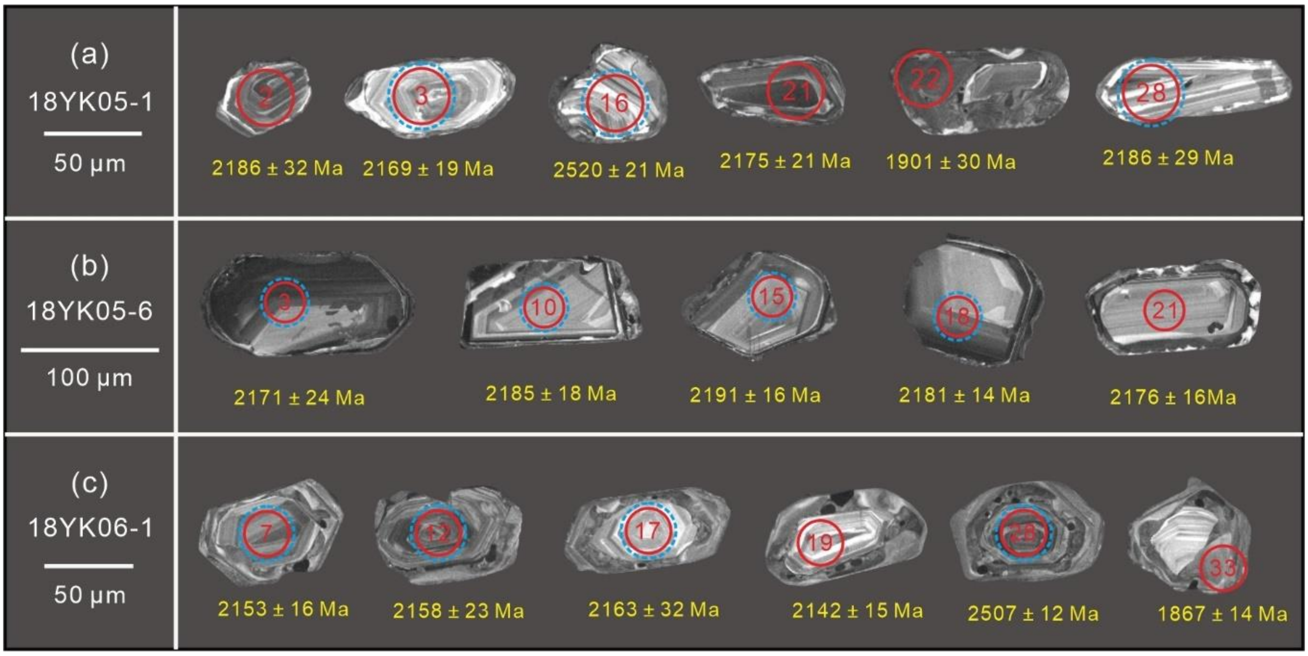

Figure 4. Representative zircon cathodoluminescence (CL) images of the felsic metavolcanic rocks. (**a**) Sample 18YK05-1; (**b**) Sample 18YK05-6; (**c**) Sample 18YK06-1. The blue dashed circle and internal red circle represent the positions of Hf isotopic and U-Pb age analyses, respectively.

As shown in the CL images (Figure 4a), zircon crystals from Sample 18YK05-1 are generally subhedral to anhedral and grey to white in color, with grain lengths of approximately 50–100 μm and length/width ratios of 1.2–2.5. Most of the zircon grains exhibit clear and well-developed oscillatory zoning, or characteristic core-rim structures (Figure 4a). Combined with their relatively high Th/U ratios of 0.47–1.18 (Supplementary Table S1), these zircon grains and cores are similar to those of felsic igneous rocks, indicating a magmatic origin. Nineteen U-Pb analysis spots on the above zircon domains yield apparent ^{207}Pb/^{206}Pb dates between 2188 $\pm$ 17 Ma and 2163 $\pm$ 24 Ma, with a weighted mean ^{207}Pb/^{206}Pb age of 2174 $\pm$ 10 Ma (n = 19, MSWD = 0.12), and all of them have concordances better than 96% and fall on or near the Concordia line (Figure 5a). Therefore, the age of 2174 $\pm$ 10 Ma represents the magma eruption age of Sample 18YK05-1. Six analyses on zircon core domains gave old apparent ^{207}Pb/^{206}Pb dates of 2529–2479 Ma, suggesting that these zircon cores could be inherited zircons derived from the Neoarchean basement rocks of the Longgang Block (Supplementary Table S1 and Figure 5a). In addition, two analyses on zircon grains or rims without obvious internal structures gave ^{207}Pb/^{206}Pb dates 1901 $\pm$ 30 Ma and 1898 $\pm$ 30 Ma, consistent with the Late Paleoproterozoic regional metamorphic event in the JLJB.

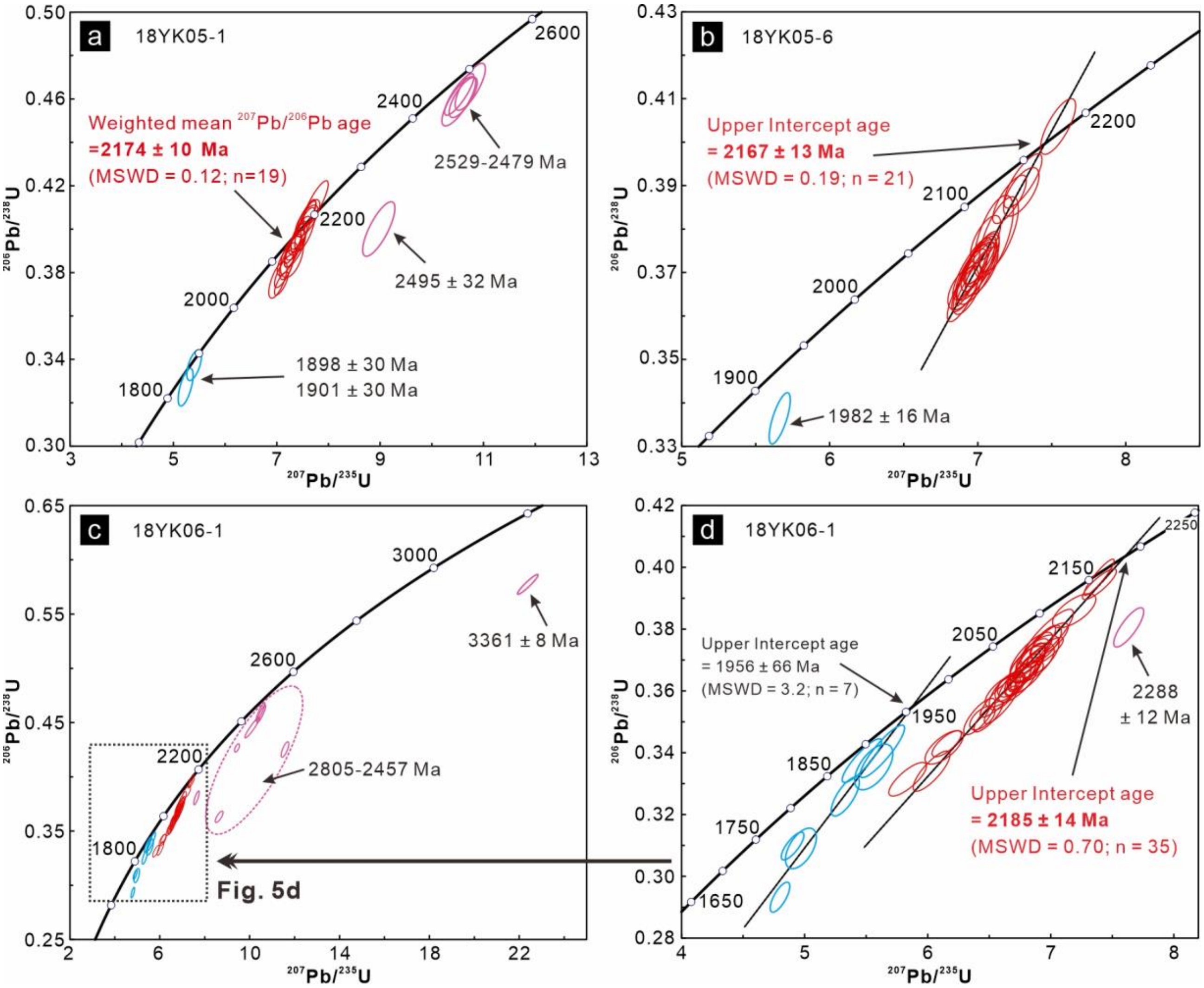

Figure 5. Zircon U-Pb Concordia diagrams of the felsic metavolcanic rocks. (**a**) Sample 18YK05-1; (**b**) Sample 18YK05-6; (**c**) Sample 18YK06-1; (**d**) Partial enlarged view of Figure 5c (Sample 18YK06-1).

Zircon grains from Sample 18YK05-6 are euhedral to subhedral crystals and black to grey in color in the CL images (Figure 4b), with grain lengths ranging from 75 to 150 μm and aspect ratios of 1.1–2.0. The majority of zircon crystals have well-developed oscillatory growth zoning, and some of them display clear core-rim textures (Figure 4b). In addition, they show relatively high and variable Th/U ratios varying from 0.13 to 0.85 (Supplementary Table S1). All of these features indicate that these zircon grains or cores have a magmatic origin. Twenty-one U-Pb analysis spots with concordances better than 95% yield apparent $^{207}Pb/^{206}Pb$ dates between 2196 ± 21 Ma and 2163 ± 14 Ma (Supplementary Table S1). They define a discordant line and give an upper intercept age of 2167 ± 13 Ma (n = 21, MSWD = 0.19), which is interpreted as the magma eruption age of Sample 18YK05-6 (Figure 5b).

Zircon crystals from Sample 18YK06-1 are irregularly shaped, grey to white in color and subhedral to anhedral in CL images (Figure 4c), with grain lengths of approximately 70–100 μm and length/width ratios ranging from 1.0 to 2.0. Most of them exhibit obvious core-rim structures with well-developed oscillatory zoned cores surrounded by structureless and blurred rims (Figure 4c). In addition, some zircon grains with no obvious core-rim structures are completely structureless or show clear oscillatory growth zoning throughout them. Thirty-five U-Pb analyses on zircon cores or domains with distinct oscillatory growth zoning, with high Th/U ratios of 0.30–1.08 (mostly >0.5), yield apparent $^{207}Pb/^{206}Pb$ dates between 2174 ± 12 Ma and 2065 ± 18 Ma (Supplementary Table S1). These analyses define a discordant line and give an upper intercept age of 2185 ± 14 Ma (n = 35, MSWD = 0.70), representing the magma eruption age of Sample 18YK06-1 (Figure 5c,d). Eight analyses yield old apparent $^{207}Pb/^{206}Pb$ dates of 3361–2288 Ma (Supplementary Table S1 and Figure 5c), which indicates that these zircon grains could be inherited in origin and derived from ancient surrounding rocks (e.g., Archean TTG rocks). In addition, seven analyses on zircon rims or domains without distinct internal structures have relatively low Th/U ratios of 0.06–0.14 (Supplementary Table S1). They yield young apparent $^{207}Pb/^{206}Pb$ dates between 1956 ± 21 Ma and 1867 ± 14 Ma, with an upper intercept age of 1956 ± 66 Ma (n = 7, MSWD = 3.2) (Supplementary Table S1 and Figure 5c,d), which represents the metamorphic age of Sample 18YK06-1.

In summary, these felsic metavolcanic rocks were formed during the early Paleoproterozoic (2185–2167 Ma) and underwent the late Paleoproterozoic regional metamorphic event (1956–1898 Ma).

5.2. Whole-Rock Geochemistry

The whole-rock major and trace element data and calculated parameters for the seven felsic metavolcanic rock samples are presented in Table 2. These samples are acid rocks with high SiO_2 (66.30–75.30 wt.%; average 69.51 wt.%) concentrations. They also contain relatively low TiO_2 (0.03–0.78 wt.%; average 0.45 wt.%), total Fe_2O_3 (tFe_2O_3; 0.55–5.03 wt.%; average 2.85 wt.%) and MnO (0.01–0.04 wt.%; average 0.02 wt.%) contents and show a large range of Al_2O_3 (10.57–17.23 wt.%), Na_2O (0.99–9.01 wt.%) and K_2O (0.04–7.15 wt.%). As shown in the protolith discrimination diagrams (Figure 6a,b) these felsic rock samples exhibit low TiO_2, Ni contents and Zr/TiO_2 ratios and mainly fall into the field of volcanic rocks rather than sedimentary rocks. In addition, most zircon grains from these samples are subhedral with the characteristics of magmatic oscillatory growth zonings, differing from detrital zircon grains from sedimentary rocks with relatively rounded shapes (Figure 4). Previous field and petrological studies also identified a suit of metavolcanic rocks (meta-rhyolites and meta-dacites) in the Li'eryu Formation, Liaohe Group [21,60,68,69]. In the geochemical classification diagrams (Figure 6c,d), these samples also mainly plot in the fields of rhyolite and dacite. Therefore, the felsic rocks in this study are a suit of metavolcanic rocks and mainly comprise meta-rhyolites and meta-dacites.

Table 2. Bulk-rock major (wt.%) and trace (ppm) element data of the felsic metavolcanic rocks in the Liaodong Peninsula of the Jiao-Liao-Ji Belt.

Sample	18YK05-2	18YK05-3	18YK05-7	18YK05-8	18YK05-9	18YK06-2	18YK06-4
SiO_2	69.95	67.24	66.43	74.31	66.54	75.30	66.77
TiO_2	0.61	0.54	0.11	0.03	0.57	0.78	0.50
Al_2O_3	12.57	11.67	17.23	14.96	14.04	10.57	15.33
tFe_2O_3	4.59	4.75	0.68	0.55	2.05	5.03	2.33
MnO	0.03	0.04	0.01	0.02	0.02	0.02	0.02
MgO	6.32	8.76	1.17	0.17	4.76	4.12	1.64
CaO	1.64	2.72	2.67	1.99	2.40	0.12	2.08
Na_2O	0.99	1.00	9.01	5.70	1.04	1.37	2.96
K_2O	0.04	0.18	0.61	1.18	7.15	1.02	6.95
P_2O_5	0.14	0.14	0.07	0.02	0.10	0.18	0.15
LOI%	2.87	2.49	1.58	0.57	0.53	0.36	0.51
Total	99.75	99.52	99.57	99.50	99.19	98.88	99.23
La	7.10	18.68	18.75	11.10	32.84	10.43	35.88
Ce	17.17	43.00	38.72	24.56	81.06	25.78	61.40
Pr	2.23	4.95	4.40	3.03	9.46	3.26	5.08
Nd	10.18	18.76	15.75	11.91	35.78	13.58	16.66
Sm	2.65	3.27	2.72	2.90	6.37	3.23	2.60
Eu	0.48	0.49	0.45	0.58	1.00	0.70	0.44

Table 2. *Cont.*

Sample	18YK05-2	18YK05-3	18YK05-7	18YK05-8	18YK05-9	18YK06-2	18YK06-4
Gd	2.88	2.92	1.95	2.93	4.93	3.15	2.48
Tb	0.45	0.42	0.24	0.49	0.68	0.51	0.34
Dy	2.92	2.64	1.25	3.17	4.03	3.28	2.13
Ho	0.63	0.54	0.23	0.62	0.79	0.68	0.47
Er	1.81	1.56	0.63	1.75	2.23	1.98	1.48
Tm	0.28	0.25	0.10	0.28	0.32	0.29	0.24
Yb	1.89	1.66	0.64	1.75	1.96	1.80	1.73
Lu	0.30	0.28	0.10	0.24	0.29	0.28	0.31
Y	16.30	14.28	7.84	20.40	18.83	16.27	15.13
tREE	50.97	99.44	85.95	65.30	181.74	68.95	131.25
LREE/HREE	3.57	8.68	15.68	4.82	10.93	4.76	13.28
$(La/Yb)_N$	2.70	8.06	20.86	4.55	12.00	4.14	14.88
δEu	0.53	0.49	0.60	0.61	0.54	0.67	0.53
δCe	1.06	1.10	1.05	1.04	1.13	1.08	1.12
Li	13.26	17.28	11.06	10.73	63.88	64.08	25.38
Sc	10.51	11.45	1.50	2.33	5.25	13.48	12.58
V	97.42	140.20	20.92	21.50	45.20	90.29	25.11
Cr	54.30	45.62	10.54	9.16	56.36	67.30	61.46
Co	5.13	7.00	3.51	3.28	4.40	6.22	2.01
Ni	21.06	19.25	4.00	3.90	22.96	25.70	21.86
Cu	0.75	0.92	9.39	12.08	4.33	1.78	4.35
Zn	53.02	81.30	34.72	35.22	37.94	16.17	32.63
Ga	15.45	16.33	18.66	16.75	18.36	17.61	24.03
Rb	1.05	9.99	15.23	17.71	148.42	149.30	75.74
Sr	187.64	148.84	1112.80	963.60	122.30	108.26	239.40
Zr	216.60	222.20	132.28	134.42	241.20	191.52	251.82
Nb	1.45	2.40	1.81	3.64	15.68	11.62	16.22
Cs	0.15	1.12	0.54	0.42	15.65	11.40	5.47
Ba	3.04	6.78	197.78	197.28	89.52	758.80	107.74
Hf	5.04	5.24	3.00	3.08	5.58	4.78	6.06
Ta	0.10	0.17	0.12	0.25	1.07	0.69	1.01
Pb	4.79	4.34	8.03	10.65	4.05	2.03	7.30
Th	11.20	11.24	4.55	2.14	13.57	7.36	14.82
U	0.60	0.71	0.69	0.68	0.91	0.73	1.65

The felsic metavolcanic rocks contain relatively low Cr (9.16–67.30 ppm; average 43.53 ppm), Co (2.01–7.00 ppm; average 4.51 ppm), and Ni (3.90–25.70 ppm; average 16.96 ppm) (Table 2). Their right-inclined chondrite-normalized REE patterns show prominent enrichments in light REEs (LREEs) and slighter enrichments in heavy REEs (HREEs), with total REE (tREE) contents of 50.97–181.74 ppm, high $(La/Yb)_N$ ratios of 2.70–20.86, and obviously negative Eu anomalies (δEu = 0.49–0.67; average 0.57) (Table 2 and Figure 7a). In the spider diagram of primitive mantle- (PM-) normalized trace elements (Figure 7b), most felsic metavolcanic rock samples are relatively enriched in large ion lithophile elements (LILEs; e.g., Rb, Ba and K), Th and U, and show negative anomalies of high field strength elements (HFSEs; e.g., Nb, Ta, Ti and P) and Sr.

5.3. Zircon Lu-Hf Isotopic Compositions

The zircon Lu-Hf isotopic results for the three dated samples (18YK05-1, 18YK05-6 and 18YK06-1) are presented in Figure 8 and Table 3. Thirty-four Lu-Hf analyses on magmatic zircon grains (2185–2167 Ma) from the three felsic metavolcanic rock samples yield $^{176}Lu/^{177}Hf$ ratios ranging from 0.000326 to 0.002066 and $^{176}Hf/^{177}Hf$ ratios ranging from 0.281430 to 0.281683 (Table 3). They display variable εHf(t) values varying from −0.70 to +9.69 (Table 3) and fall into the field between the depleted mantle (DM) evolutionary line and chondrite uniform reservoir (CHUR) line in the εHf(t) versus age diagram (Figure 8). The calculated two-stage Hf model ages (T_{DM2}) for the felsic metavolcanic rocks range from

2903 to 2152 Ma (Table 3). In addition, eleven analyses on inherited zircon grains, with ancient apparent $^{207}Pb/^{206}Pb$ ages of 3361–2288 Ma, have $^{176}Lu/^{177}Hf$ ratios of 0.000809 to 0.001462, $^{176}Hf/^{177}Hf$ ratios of 0.281010 to 0.281539, and a large range of εHf(t) values (−1.85 to +14.99) (Table 3).

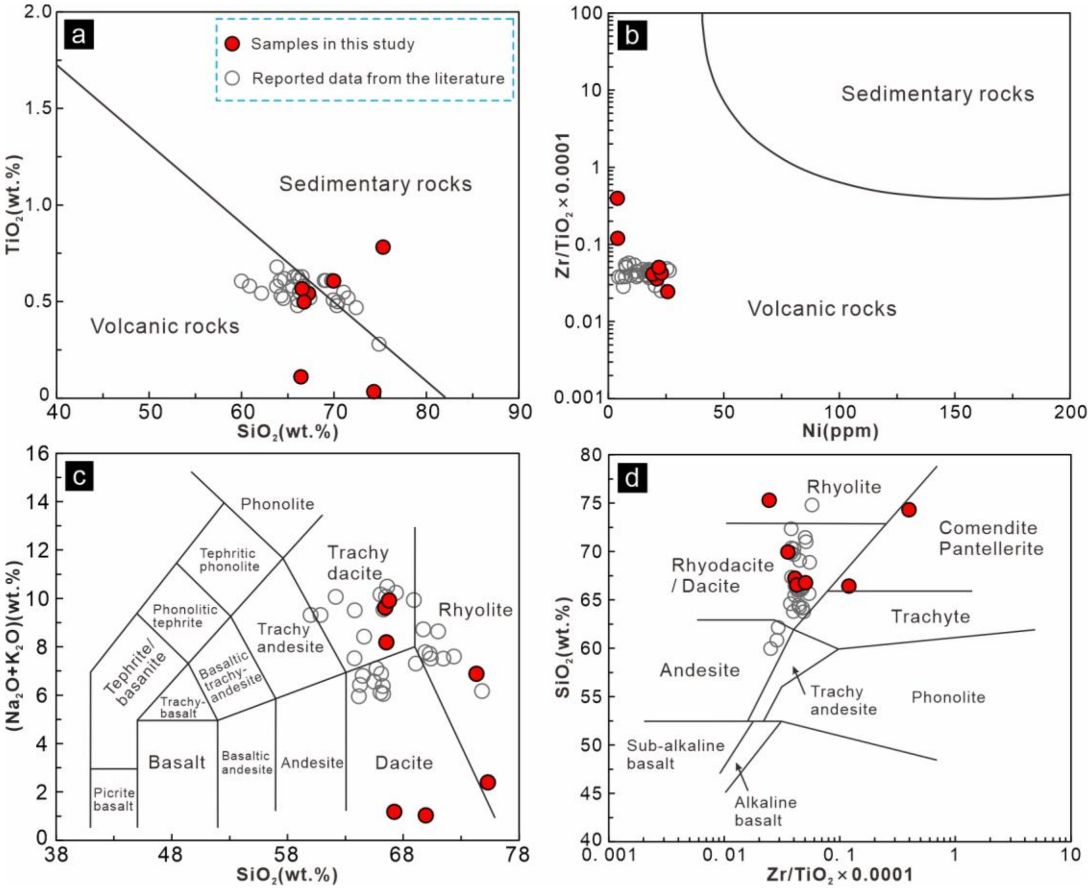

Figure 6. Geochemical classification diagrams of the felsic metavolcanic rocks. (**a**) TiO_2 versus SiO_2 diagram [70]; (**b**) $Zr/TiO_2 \times 0.0001$ versus Ni diagram [71]; (**c**) ($Na_2O + K_2O$) versus SiO_2 diagram [72]; (**d**) SiO_2 versus $Zr/TiO_2 \times 0.0001$ diagram [73]. Reported data of the felsic metavolcanic rocks are from [21,60,68,69].

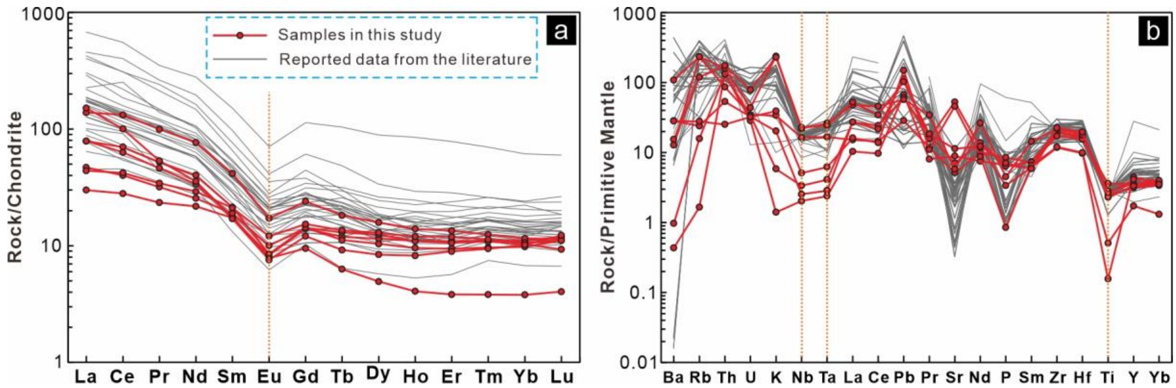

Figure 7. (**a**) Chondrite-normalized REE pattern diagram; (**b**) Primitive mantle-normalized spider diagram. Reported data of the felsic metavolcanic rocks are from [21,60,68,69]. The normalized values are from [74].

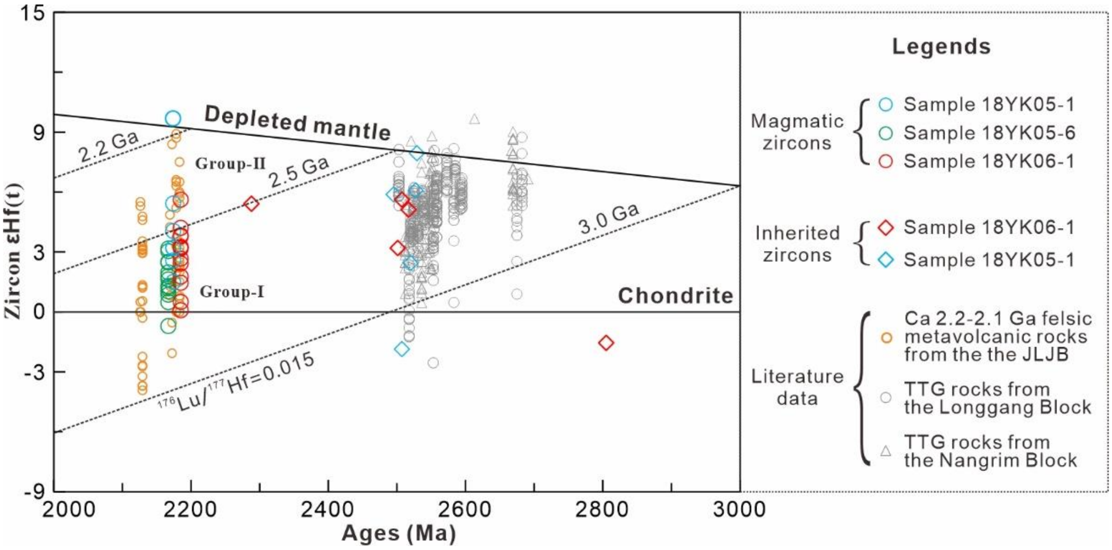

Figure 8. The εHf(t) versus age diagram of the felsic metavolcanic rocks. Reported Hf isotopic data of the felsic metavolcanic rocks are from [60,68]. Reported Hf isotopic data of the TTG rocks in the Longgang Block are from [52,53,75,76]. Reported Hf isotopic data of the TTG rocks in the Nangrim Block are from [57].

Table 3. Zircon Hf isotopic data of the felsic metavolcanic rocks in the Liaodong Peninsula of the Jiao-Liao-Ji Belt.

Sample	t (Ma)	^{176}Lu/^{177}Hf	2σ	^{176}Hf/^{177}Hf	2σ	εHf(t)	T_{DM1} (Ma)	T_{DM2} (Ma)
				Sample 18YK05-1				
18YK05-1-01	2527	0.000914	0.000065	0.281383	0.000027	6.08	2603	2649
18YK05-1-03	2174	0.000326	0.000006	0.281683	0.000028	9.69	2160	2152
18YK05-1-07	2174	0.001437	0.000045	0.281609	0.000020	5.43	2326	2415
18YK05-1-10	2174	0.000838	0.000013	0.281546	0.000018	4.05	2377	2500
18YK05-1-13	2507	0.000872	0.000015	0.281171	0.000024	−1.85	2888	3118
18YK05-1-14	2495	0.001190	0.000016	0.281411	0.000021	5.89	2584	2636
18YK05-1-16	2520	0.000809	0.000005	0.281281	0.000018	2.45	2735	2865
18YK05-1-17	2174	0.001382	0.000019	0.281496	0.000015	1.50	2479	2657
18YK05-1-24	2174	0.000809	0.000010	0.281521	0.000015	3.22	2409	2551
18YK05-1-26	2174	0.000820	0.000011	0.281503	0.000015	2.57	2434	2591
18YK05-1-27	2529	0.001021	0.000007	0.281440	0.000036	7.95	2533	2536
18YK05-1-28	2174	0.002066	0.000054	0.281572	0.000033	3.19	2418	2553
				Sample 18YK05-6				
18YK05-6-01	2167	0.000842	0.000014	0.281487	0.000017	1.80	2457	2720
18YK05-6-02	2167	0.001164	0.000021	0.281430	0.000018	−0.70	2556	2903
18YK05-6-03	2167	0.001750	0.000002	0.281544	0.000015	2.52	2436	2669
18YK05-6-04	2167	0.001029	0.000032	0.281529	0.000016	3.04	2411	2630
18YK05-6-05	2167	0.001356	0.000029	0.281471	0.000018	0.49	2513	2817
18YK05-6-06	2167	0.001740	0.000023	0.281529	0.000018	1.99	2457	2709
18YK05-6-09	2167	0.001099	0.000008	0.281476	0.000016	1.03	2489	2777
18YK05-6-10	2167	0.001206	0.000035	0.281484	0.000018	1.17	2485	2767
18YK05-6-13	2167	0.000927	0.000029	0.281529	0.000019	3.17	2405	2620
18YK05-6-15	2167	0.001490	0.000013	0.281498	0.000019	1.26	2484	2761
18YK05-6-16	2167	0.001339	0.000026	0.281481	0.000018	0.87	2497	2789
18YK05-6-17	2167	0.000959	0.000016	0.281477	0.000014	1.30	2478	2757
18YK05-6-18	2167	0.000960	0.000013	0.281487	0.000016	1.63	2465	2733
18YK05-6-19	2167	0.000727	0.000015	0.281501	0.000017	2.47	2431	2671

Table 3. *Cont.*

Sample	t (Ma)	$^{176}Lu/^{177}Hf$	2σ	$^{176}Hf/^{177}Hf$	2σ	εHf(t)	T_{DM1} (Ma)	T_{DM2} (Ma)
Sample 18YK06-1								
18YK06-1-04	2185	0.001448	0.000052	0.281558	0.000016	3.84	2398	2521
18YK06-1-05	2185	0.001308	0.000018	0.281447	0.000018	0.09	2543	2752
18YK06-1-06	2185	0.001060	0.000012	0.281509	0.000017	2.67	2441	2593
18YK06-1-07	2185	0.001071	0.000007	0.281592	0.000018	5.62	2327	2412
18YK06-1-10	2185	0.001233	0.000007	0.281548	0.000017	3.79	2399	2525
18YK06-1-11	2185	0.001376	0.000013	0.281536	0.000016	3.17	2424	2563
18YK06-1-12	2185	0.000958	0.000007	0.281479	0.000015	1.77	2475	2649
18YK06-1-14	2501	0.000898	0.000005	0.281318	0.000015	3.21	2691	2805
18YK06-1-17	2185	0.001109	0.000008	0.281477	0.000017	1.47	2488	2668
18YK06-1-26	2805	0.001231	0.000045	0.281010	0.000017	−1.55	3135	3329
18YK06-1-28	2507	0.000990	0.000009	0.281387	0.000023	5.63	2603	2661
18YK06-1-32	3361	0.001162	0.000008	0.281118	0.000027	14.99	2982	2758
18YK06-1-34	2288	0.001462	0.000005	0.281539	0.000018	5.42	2425	2504
18YK06-1-36	2185	0.001016	0.000016	0.281550	0.000016	4.21	2381	2499
18YK06-1-37	2185	0.001163	0.000008	0.281530	0.000016	3.27	2418	2557
18YK06-1-39	2185	0.001575	0.000026	0.281524	0.000025	2.43	2454	2608
18YK06-1-40	2517	0.001081	0.000014	0.281370	0.000018	5.12	2632	2700
18YK06-1-45	2185	0.001735	0.000051	0.281476	0.000016	0.51	2531	2726
18YK06-1-46	2185	0.001551	0.000048	0.281545	0.000017	3.22	2423	2560

The present-day $^{176}Hf/^{177}Hf$ and $^{176}Lu/^{177}Hf$ ratios are 0.282772 and 0.0332 for the chondrite, and 0.28325 and 0.0384 for depleted mantle. The $^{176}Lu/^{177}Hf$ ratio of the average continental crust is 0.015. The decay constant of ^{176}Lu is 6.54×10^{-12} a^{-1}.

6. Discussion

6.1. Early Paleoproterozoic (ca. 2.2–2.1 Ga) Magmatism in the Liaodong Peninsula of the JLJB

The early Paleoproterozoic (concentrated at ca. 2.2–2.1 Ga) is one of the most developed periods of magmatic activity in the JLJB [24]. A large number of ca. 2.2–2.1 Ga igneous rocks are widely distributed in the Liaodong Peninsula of the JLJB [21,22,31,33,38,44,45,60,61,68] (Figure 1b). They are mainly composed of three lithological units, including meta-volcanic rock, granitic intrusion, and mafic intrusion. Characteristically, the meta-volcanic rocks and granitic intrusions were mainly formed at ca. 2205–2150 Ma and ca. 2185–2150 Ma, respectively, but the mafic intrusions were emplaced relatively late (concentrated at ca. 2160–2100 Ma) (Figure 9). The meta-volcanic sequences are mainly outcropped in the North and South Liaohe Groups and characterized by bimodal volcanic rocks [21,40,77,78]. They display various lithologies, mainly composed of meta-rhyolite, meta-dacite, fine-grained gneiss, amphibolite, and meta-basalt. The granitic intrusions, also known as Liaoji granites, are generally outcropped as gneissic plutons in the eastern Liaoning and southern Jilin areas [22] (Figure 1b). The Liaoji granites with typical A-type granite affinity and bimodal volcanic sequences are widely regarded as the products of intra-continental rift [21,22,79,80]. Voluminous meta-mafic intrusions are distributed in the northern part of the Liaodong Peninsula (i.e., Haicheng and Helan areas), and minor intrusions are distributed in the Xiuyan and Kuandian areas [31,38,44,46,79] (Figure 1b). These mafic intrusions, comprising meta-gabbro, meta-diabase, and amphibolite, were thought to show close genetic association with extensional tectonic regimes (e.g., intra-continental rift and back-arc basin) [31,38,44,46,79].

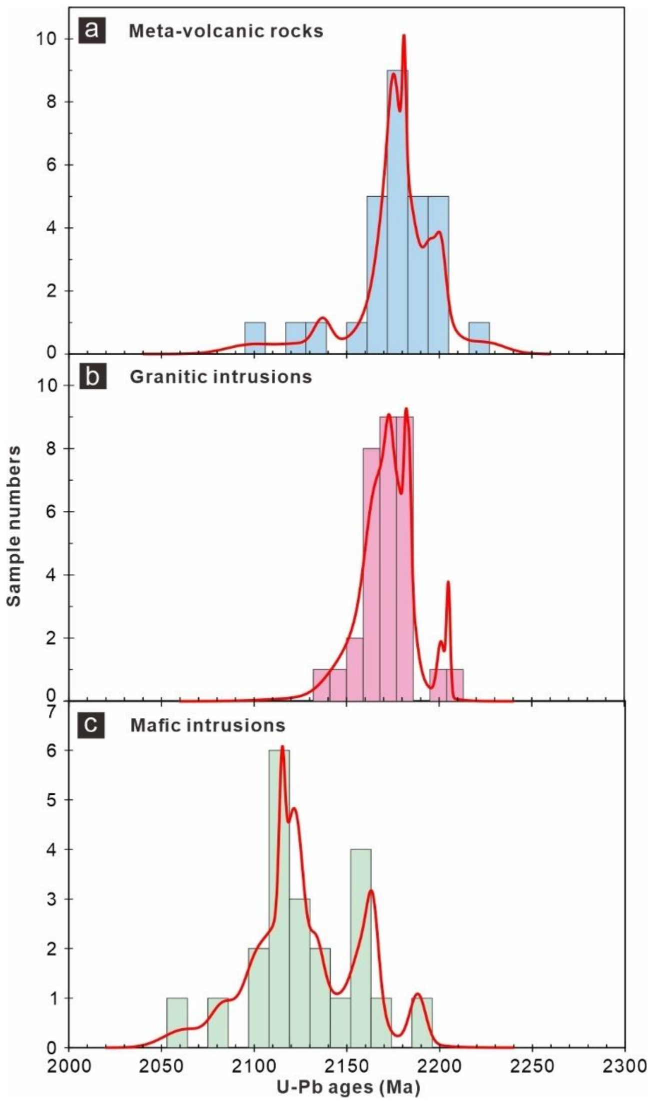

Figure 9. U-Pb age histograms of the early Paleoproterozoic magmatic rocks in the Liaodong Peninsula of the JLJB. Data of the metavolcanic rocks are from [21,27,39,60,68,69,81–84] and this study. Data of the granitic intrusions are from [21,22,45,68,77,80,81,84–89]. Data of the mafic intrusions are from [31,33,36,38,44,46].

6.2. Petrogenesis

The early Paleoproterozoic felsic metavolcanic rocks in this study underwent low-grade metamorphism as a result of a late Paleoproterozoic tectothermal event. Therefore, it is necessary to evaluate the metamorphism effects on their bulk-rock major and trace element data. All of the samples contain lower loss on ignition (LOI) contents (0.36–2.87 wt.%; average 1.27 wt.%) (Table 2), suggesting that the effects of low-grade metamorphism on geochemical compositions could be negligible. Such an explanation is also supported by the lack of obvious Ce anomalies (δCe = 1.04–1.13; average 1.08) in all samples (Table 2 and Figure 7a). Therefore, the geochemical data of felsic metavolcanic rocks in this study can be used to effectively discuss and trace their petrogenesis and tectonic implications.

The felsic metavolcanic rock samples show relatively variable tREE contents (50.97–181.74 ppm), $(La/Yb)_N$ ratios (2.70–20.86), and negative Eu anomalies (δEu = 0.49–0.67) (Table 2), which implies that they could experience a fractional crystallization process. The negative correlation between SiO_2 and Al_2O_3 suggests the felsic metavolcanic rocks experienced the plagioclase fractionation (Figure 10a), which is also consistent with their negative Eu anomalies in the REE pattern diagram (Figure 7a). These samples exhibit a negative evolutionary trend between Er and Dy (Figure 10b), which suggests the hornblende fractionation [90]. Such an explanation is supported by the decrease in V contents with decreasing Cr concentrations [91] (Figure 10c). However, the lack of an obvious evolutionary trend between Th and V implies that the biotite fractionation process is negligible [90] (Figure 10d). In addition, their relatively variable tFe_2O_3 (0.55–5.03 wt.%) and TiO_2 (0.03–0.78 wt.%) abundances are indicative of Fe-Ti oxide (e.g., magnetite and titanite) accumulation. Therefore, the felsic metavolcanic rocks in this study experienced a certain degree of fractional crystallization.

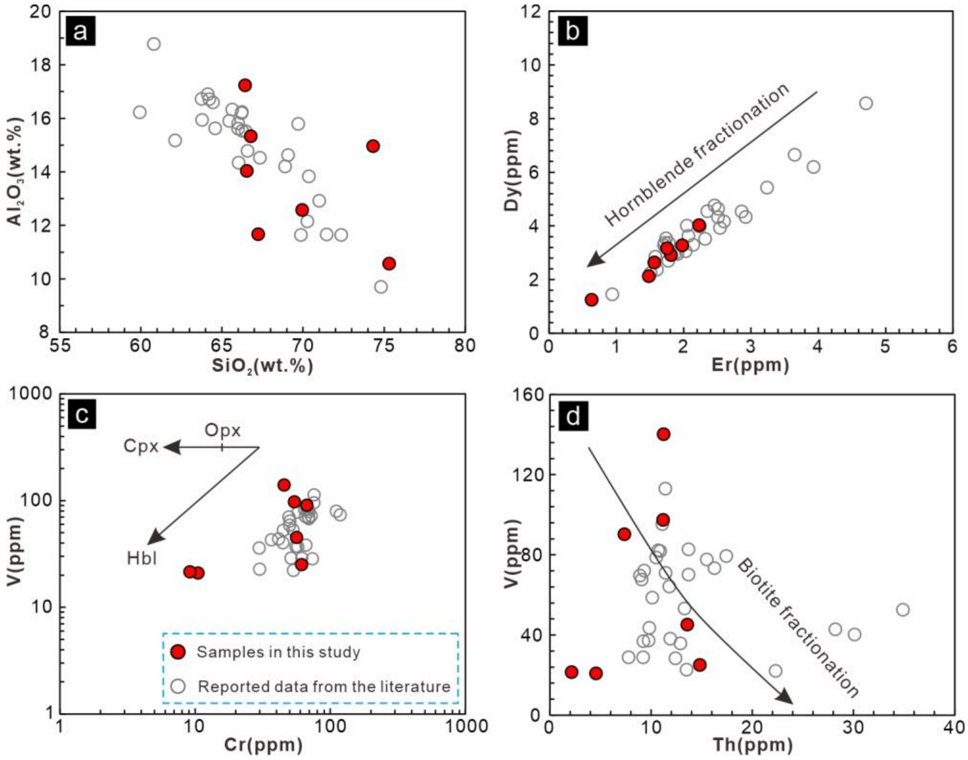

Figure 10. (**a**) Al_2O_3 versus SiO_2 diagram; (**b**) Dy versus Er diagram; (**c**) V versus Cr diagram [91]; (**d**) V versus Th diagram. Reported data of the felsic metavolcanic rocks are from [21,60,68,69].

The felsic metavolcanic rocks lack the mafic enclaves, which indicates that these samples may not have been contaminated by mantle-derived materials. Such an interpretation is also consistent with their low TiO_2 (0.03–0.78 wt.%), tFe_2O_3 (0.55–5.03 wt.%), Cr (9.16–67.30 ppm), Co (2.01–7.00 ppm), and Ni (3.90–25.70 ppm) (Table 2). The petrogenesis of felsic magmatism generally includes two main mechanisms: (1) fractional crystallization of mantle-derived magmas [91–95] and (2) partial melting of crustal materials [60,68,96–99]. As discussed above, although the primary magma of felsic metavolcanic rocks in this study inevitably experienced a certain degree of fractional crystallization during the later stage of magma eruption to the surface, their petrogenesis mechanism could not be the fractional crystallization of mantle-derived magmas. Firstly, the differentiation process of basaltic magmas will produce a complete set of magmatic evolutionary sequences, including basaltic, andesitic and rhyolitic magmatisms. However, the early Paleoproterozoic meta-volcanic sequences in the JLJB are characterized by bimodal volcanic rocks [21,40,77,78]. Secondly, multiple positive correlations between La contents and La/Sm, La/Yb, La/Hf ratios strongly suggest that the petrogenesis of the felsic metavolcanic rocks is mainly controlled by the partial melting process rather than fractional crystallization (Figure 11a–c), which is also supported by the positive correlation between Ce contents and Ce/Zr ratios (Figure 11d). These rock samples contain relatively high SiO_2 (66.30–75.30 wt.%) and low tFe_2O_3 (0.55–5.03 wt.%), MgO (0.17–8.76 wt.%), Cr (9.16–67.30 ppm), Co (2.01–7.00 ppm) and Ni (3.90–25.70 ppm) contents (Table 2), suggesting that they were mainly derived from partial melting of crustal rocks rather than mantle peridotite. Thirdly, felsic magmatism generated by the fractional crystallization of mantle-derived magmas generally exhibits depleted and homogeneous zircon Hf compositions. Nevertheless, the zircon samples from the felsic metavolcanic rocks in the Liaodong Peninsula of the JLJB exhibit a large range of εHf(t) values, and some samples even fall below the CHUR line and show enriched zircon Hf compositions (Figure 8). Therefore, the fractional crystallization mechanism may not play a major role in geochemical compositions. In summary, the petrogenesis of the felsic metavolcanic rocks in this study are most likely the mechanism (2): partial melting of pre-existing crustal materials.

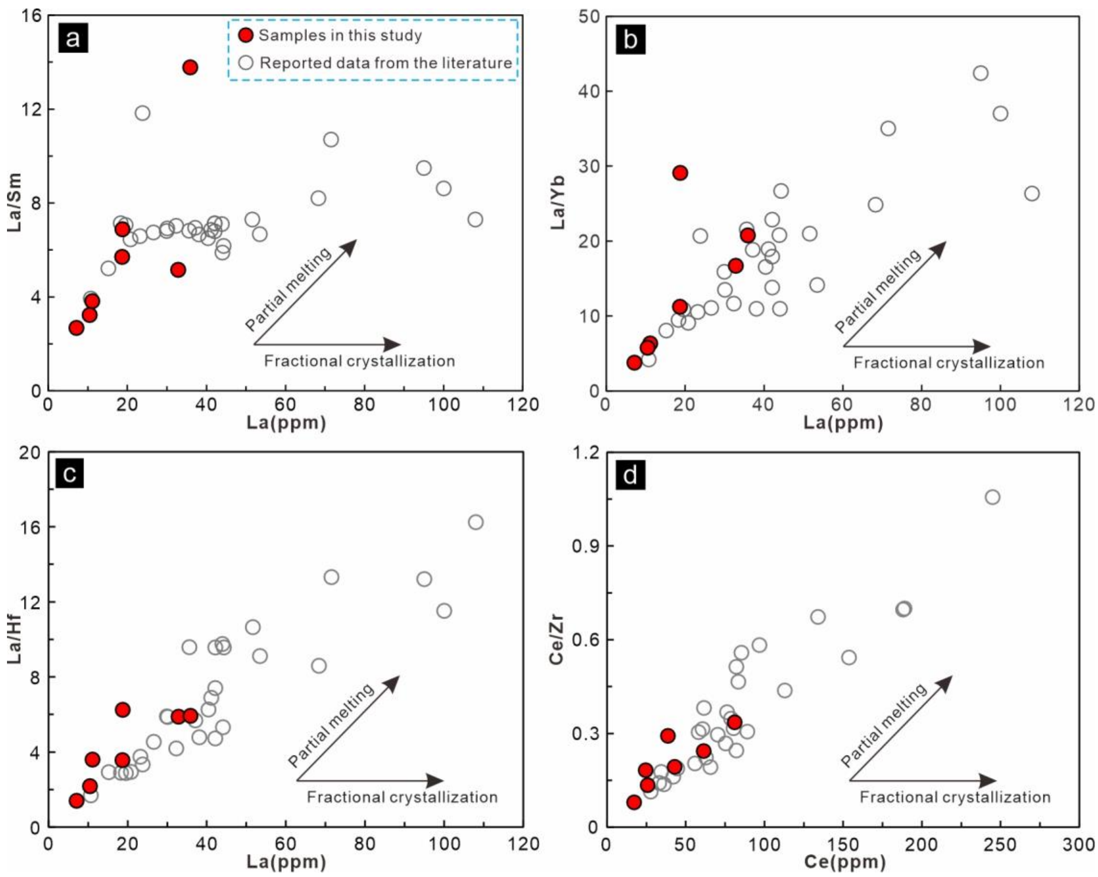

Figure 11. (**a**) La/Sm versus La diagram; (**b**) La/Yb versus La diagram; (**c**) La/Hf versus La diagram; (**d**) Ce/Zr versus Ce diagram. Reported data of the felsic metavolcanic rocks are from [21,60,68,69].

Zircon CL images and U-Pb geochronological results reveal that the felsic metavolcanic rocks of this study contain many inherited magmatic zircon grains with ancient apparent $^{207}Pb/^{206}Pb$ ages ranging from 3361 ± 8 Ma to 2288 ± 12 Ma (concentrated at the Neoarchean) (Supplementary Table S1 and Figure 4a,c). Therefore, the Neoarchean TTG rocks, accounting for the majority of continental crust rocks in the Archean Longgang and Nangrim blocks [52,53,57], are potential protoliths for the felsic metavolcanic rocks. In this study, we collected zircon Hf isotopic data from reported early Paleoproterozoic felsic metavolcanic rocks in the Liaodong Peninsula and Neoarchean TTG rocks in the Longgang and Nangrim blocks. Zircon grains from the early Paleoproterozoic felsic metavolcanic rocks exhibit heterogeneous zircon Hf isotopic compositions with a broad range of εHf(t) values (approximately −4 to +9) (Figure 8). They can be divided into two groups based on their different εHf(t) values and T_{DM2} ages. Zircons of the Group-I show similar ancient T_{DM2} ages of ca. 3.0–2.5 Ga and low εHf(t) values (about −4 to +4), which indicates that the felsic metavolcanic rocks could be derived from partial melting of ancient Archean

TTG rocks. Such an explanation is also supported by their T_{DM2} ages and evolutionary trends being similar to those of Neoarchean TTG rocks (Figure 8). Differently, zircons of the Group-II are close to the DM evolutionary line with higher εHf(t) values (about +4 to +9) and younger T_{DM2} ages (ca. 2.5–2.2 Ga), which suggests that juvenile mafic materials in the lower crust could be another source for the felsic metavolcanic rocks (Figure 8). In summary, the early Paleoproterozoic felsic metavolcanic rocks in the Liaodong Peninsula of the JLJB were most likely derived from partial melting of Archean TTG rocks and juvenile crustal materials.

6.3. Tectonic Implications

The early Paleoproterozoic tectonic evolution of the JLJB has long been controversial [13,14,24,32,33]. Therefore, contemporaneous magmatic rocks can provide valuable insights into this issue. There is a view that ca. 2.2–2.1 Ga metavolcanic sequences, mafic and granitic intrusions with arc-type geochemical characteristics (enrichment in LILE and depletion in HFSE) were considered to be associated with magmatic arc-related environments [27,33,38,46,60,61,68]. However, many studies revealed that the JLJB went through an intra-continental rift system during the early Paleoproterozoic. Firstly, the Longgang and Nangrim blocks on both sides of the JLJB have similar Archean basement rocks geochemically and geochronologically [3,40], which indicates that the two blocks previously belonged to a unified continent. Secondly, the existence of regional large-scale mafic dykes generally represents a crustal extension tectonic regime. In the whole JLJB, abundant ca. 2.2–2.1 Ga mafic intrusions were identified in southern Jilin Province and on the Liaodong Peninsula [31,38,44,46,79]. Thirdly, the metavolcanic sequences in the JLJB are mainly composed of bimodal volcanic rocks [21,40,77,78], which indicates that the JLJB experienced an intra-continental rift rather than magmatic arc during the early Paleoproterozoic. Fourthly, a large number of Liaoji granites with an affinity of A-type granite also suggest an intra-continental rift setting [21,22,43,45,80]. Finally, the absence of coeval typical arc magmatism in the JLJB could be in disagreement with an arc-related setting [3,18,21,22]. Therefore, these lines of evidence indicate that the JLJB most likely went through an intra-continental rift during the early Paleoproterozoic. In this study, the ca. 2185–2167 Ma felsic metavolcanic rocks are closely related to A-type granite and metavolcanic rocks in the spatial and temporal distribution. It can be inferred that they were also generated in an intra-continental rift setting.

Liu et al. (2020) [22] identified a suit of synchronous A-type and adakitic granites, which were formed in an intra-continental rift trigged by lithospheric delamination at ca. 2.2 Ga. Generally, the lithospheric delamination could result in the decompression melting and upwelling of asthenosphere mantle and generate the mafic volcanic and intrusive rocks in the JLJB. Meanwhile, the upwelling of hyperthermal mantle-derived magmas will further induce the appearance of initial rift and partial melting of crustal rocks and produce the numerous A-type Liaoji granites and felsic volcanic rocks of this study. Such a delamination-rift model can effectively explain the special early Paleoproterozoic lithological assemblages in the JLJB.

A further extension of continental rift would have resulted in an initial ocean basin and separated unified Eastern Block into two continental blocks (i.e., the Longgang and Nangrim blocks). A subsequent regional high-grade tectothermal event at ca. 1.95–1.85 Ga resulted in the collision between the Longgang and Nangrim blocks [15–17,26,29,63]. Correspondingly, the felsic metavolcanic rocks in this study also recorded metamorphic ages of 1956–1898 Ma (Figure 5). Notably, increasing studies from metamorphic geology, especially the discovery of a high-pressure mafic/pelitic granulite with a clockwise P-T-t path, strongly revealed that the JLJB experienced oceanic subduction before the final collision [16,17,26,63]. Therefore, the most likely tectonic scenario is that the JLJB went through an intra-continental rift system during the early Paleoproterozoic (ca. 2.2–2.1 Ga), followed by a transition phase from rift to oceanic subduction, and later a continent–continent collision at ca. 1.95–1.85 Ga [3,21,22,31].

7. Conclusions

1. The felsic metavolcanic rocks in the Liaodong Peninsula were erupted at 2185–2167 Ma and underwent a late metamorphic event at 1956–1898 Ma.
2. Geochemical and isotopic results suggest that the felsic metavolcanic rocks were derived from partial melting of Archean TTG rocks and Paleoproterozoic juvenile lower crustal materials.
3. The JLJB most likely experienced an intra-continental rift at ca. 2.2–2.1 Ga.

Supplementary Materials: The following supporting information can be downloaded at: https://www.mdpi.com/article/10.3390/min13091168/s1, Table S1: Zircon U-Pb data for the felsic metavolcanic rocks in the Liaodong Peninsula of the Jiao-Liao-Ji Belt.

Author Contributions: Conceptualization, C.C., J.L. and J.Z.; methodology, C.C., J.L. and H.Z.; software, C.C.; validation, C.C.; formal analysis, C.C., H.Z. and Y.C.; investigation, C.C., J.L., H.Z., Y.C., X.W., Z.L. and H.Y.; data curation, C.C.; writing—original draft preparation, C.C.; writing—review and editing, J.L. and J.Z.; supervision, J.L. and J.Z.; project administration, J.L. and J.Z.; funding acquisition, J.L. and J.Z. All authors have read and agreed to the published version of the manuscript.

Funding: This research was funded by the National Natural Science Foundation of China (Grant Nos. 42025204 and 42172212).

Data Availability Statement: Not applicable.

Acknowledgments: We sincerely thank the Academic Editor and three anonymous reviewers for their constructive and helpful comments. We also thank the Managing Editor and Assistant Editor very much for their editorial work.

Conflicts of Interest: The authors declare no conflict of interest.

References

1. Zhao, G.C.; Sun, M.; Wilde, S.A.; Li, S.Z. Late Archean to Paleoproterozoic evolution of the North China Craton: Key issues revisited. *Precambrian Res.* **2005**, *136*, 177–202. [CrossRef]
2. Zhao, G.C.; Wilde, S.A.; Guo, J.H.; Cawood, P.A.; Sun, M.; Li, X.P. Single zircon grains record two Paleoproterozoic collisional events in the North China Craton. *Precambrian Res.* **2010**, *177*, 266–276. [CrossRef]
3. Zhao, G.C.; Cawood, P.A.; Li, S.Z.; Wilde, S.A.; Sun, M.; Zhang, J.; He, Y.H.; Yin, C.Q. Amalgamation of the North China Craton: Key issues and discussion. *Precambrian Res.* **2012**, *222–223*, 55–76. [CrossRef]
4. Santosh, M.; Wilde, S.A.; Li, J.H. Timing of Paleoproterozoic ultrahigh-temperature metamorphism in the North China Craton: Evidence from shrimp U-Pb zircon geochronology. *Precambrian Res.* **2007**, *159*, 178–196. [CrossRef]
5. Zhai, M.G.; Santosh, M. The early Precambrian odyssey of North China Craton: A synoptic overview. *Gondwana Res.* **2011**, *20*, 6–25. [CrossRef]
6. Zhai, M.G.; Santosh, M. Metallogeny of the North China Craton: Link with secular changes in the evolving Earth. *Gondwana Res.* **2013**, *24*, 275–297. [CrossRef]
7. Wan, Y.S.; Liu, D.Y.; Nutman, A.P.; Zhou, H.Y.; Dong, C.Y.; Yin, X.Y.; Ma, M.Z. Multiple 3.8-3.1 Ga tectono-magmatic events in a newly discovered area. *J. Asian Earth Sci.* **2012**, *54–55*, 18–30. [CrossRef]
8. Wan, Y.S.; Xie, S.W.; Yang, C.H.; Kröner, A.; Ma, M.Z.; Dong, C.Y.; Du, L.L.; Xie, H.Q.; Liu, D.Y. Early Neoarchean (~2.7 Ga) tectono-thermal events in the North China Craton: A synthesis. *Precambrian Res.* **2014**, *247*, 45–63. [CrossRef]
9. Kusky, T.M.; Polat, A.; Windley, B.F.; Burke, K.C.; Dewey, J.F.; Kidd, W.S.F.; Maruyama, S.; Wang, J.P.; Deng, H.; Wang, Z.S.; et al. Insights into the tectonic evolution of the North China Craton through comparative tectonic analysis: A record of outward growth of Precambrian continents. *Earth-Sci. Rev.* **2016**, *162*, 387–432. [CrossRef]
10. Zhang, J.; Zhao, G.C.; Li, S.Z.; Sun, M.; Chan, L.S.; Shen, W.L.; Liu, S.W. Structural pattern of the Wutai Complex and its constraints on the tectonic framework of the Trans-North China Orogen. *Precambrian Res.* **2012**, *222–223*, 212–229. [CrossRef]
11. Zhang, J.; Zhao, G.C.; Shen, W.L.; Li, S.Z.; Sun, M. Aeromagnetic study of the Hengshan–Wutai–Fuping region: Unraveling a crustal profile of the Paleoproterozoic Trans-North China Orogen. *Tectonophysics* **2015**, *662*, 208–218. [CrossRef]
12. Yin, C.Q.; Zhao, G.C.; Wei, C.J.; Sun, M.; Guo, J.H.; Zhou, X.W. Metamorphism and partial melting of high-pressure pelitic granulites from the Qianlishan Complex: Constraints on the tectonic evolution of the Khondalite Belt in the North China Craton. *Precambrian Res.* **2014**, *242*, 172–186. [CrossRef]
13. Li, S.Z.; Zhao, G.C.; Sun, M.; Han, Z.Z.; Hao, D.F.; Luo, Y.; Xia, X.P. Deformation history of the Paleoproterozoic Liaohe Group in the Eastern Block of the North China Craton. *J. Asian Earth Sci.* **2005**, *24*, 659–674. [CrossRef]
14. Li, S.Z.; Zhao, G.C.; Santosh, M.; Liu, X.; Dai, L.M.; Suo, Y.H.; Tam, P.Y.; Song, M.C.; Wang, P.C. Paleoproterozoic structural evolution of the southern segment of the Jiao-Liao-Ji belt, North China Craton. *Precambrian Res.* **2012**, *200–203*, 59–73. [CrossRef]

15. Tam, P.Y.; Zhao, G.C.; Sun, M.; Li, S.Z.; Iizuka, Y.; Ma, G.S.K.; Yin, C.Q.; He, Y.H.; Wu, M.L. Metamorphic P-T path and tectonic implications of medium-pressure pelitic granulites from the Jiaobei massif in the Jiao-Liao-Ji Belt, North China Craton. *Precambrian Res.* **2012**, *220–221*, 177–191. [CrossRef]
16. Tam, P.Y.; Zhao, G.C.; Zhou, X.W.; Sun, M.; Guo, J.H.; Yin, C.Q.; Wu, M.L.; He, Y.H. Metamorphic P-T path and implications of high-pressure pelitic granulites from the Jiaobei massif in the Jiao-Liao-Ji Belt, North China Craton. *Gondwana Res.* **2012**, *22*, 104–117. [CrossRef]
17. Tam, P.Y.; Zhao, G.C.; Zhou, X.W.; Guo, J.H.; Sun, M.; Li, S.Z.; Yin, C.Q.; Wu, M.L. Petrology and metamorphic P-T path of high-pressure mafic granulites from the Jiaobei massif in the Jiao-Liao-Ji Belt, North China Craton. *Lithos* **2012**, *155*, 94–109. [CrossRef]
18. Liu, F.L.; Liu, P.H.; Wang, F.; Liu, C.H.; Cai, J. Progresses and overviews of voluminous meta-sedimentary series within the Paleoproterozoic Jiao-Liao-Ji orogenic/mobile belt, North China Craton. *Acta Petrol. Sin.* **2015**, *31*, 2816–2846. (In Chinese with English Abstract)
19. Tian, Z.H.; Liu, F.L.; Windley, B.F.; Liu, P.H.; Wang, F.; Liu, C.H.; Wang, W.; Cai, J.; Xiao, W.J. Polyphase structural deformation of low- to medium-grade metamorphic rocks of the Liaohe Group in the Jiao-Liao-Ji Orogenic Belt, North China Craton: Correlations with tectonic evolution. *Precambrian Res.* **2017**, *303*, 641–659. [CrossRef]
20. Zou, Y.; Zhai, M.G.; Santosh, M.; Zhou, L.G.; Zhao, L.; Lu, J.S.; Shan, H.X. High-pressure pelitic granulites from the Jiao-Liao-Ji Belt, North China Craton: A complete P-T path and its tectonic implications. *J. Asian Earth Sci.* **2017**, *134*, 103–121. [CrossRef]
21. Liu, J.; Zhang, J.; Liu, Z.H.; Yin, C.Q.; Zhao, C.; Li, Z.; Yang, Z.J.; Dou, S.Y. Geochemical and geochronological study on the Paleoproterozoic rock assemblage of the Xiuyan region: New constraints on an integrated rift-and- collision tectonic process involving the evolution of the Jiao-Liao-Ji Belt, North China Craton. *Precambrian Res.* **2018**, *310*, 179–197. [CrossRef]
22. Liu, J.; Zhang, J.; Yin, C.Q.; Cheng, C.Q.; Liu, X.G.; Zhao, C.; Chen, Y.; Wang, X. Synchronous A-type and adakitic granitic magmatism at ca. 2.2 Ga in the Jiao–Liao–Ji belt, North China Craton: Implications for rifting triggered by lithospheric delamination. *Precambrian Res.* **2020**, *342*, 105629. [CrossRef]
23. Liu, J.; Zhang, J.; Liu, Z.H.; Yin, C.Q.; Xu, Z.Y.; Cheng, C.Q.; Zhao, C.; Wang, X. Late Paleoproterozoic crustal thickening of the Jiao–Liao–Ji belt, North China Craton: Insights from ca. 1.95–1.88 Ga syn-collisional adakitic granites. *Precambrian Res.* **2021**, *355*, 106120. [CrossRef]
24. Xu, W.; Liu, F.L. Geochronological and geochemical insights into the tectonic evolution of the Paleoproterozoic Jiao-Liao-Ji belt. Sino-Korean Craton. *Earth-Sci. Rev.* **2019**, *193*, 162–198. [CrossRef]
25. Luo, Y.; Sun, M.; Zhao, G.C.; Li, S.Z.; Xu, P.; Ye, K.; Xia, X.P. LA–ICP–MS U-Pb zircon ages of the Liaohe Group in the Eastern Block of the North China Craton: Constraints on the evolution of the Jiao–Liao–Ji Belt. *Precambrian Res.* **2004**, *134*, 349–371. [CrossRef]
26. Zhou, X.W.; Zhao, G.C.; Wei, C.J.; Geng, Y.S.; Sun, M. Metamorphic evolution and Th-U-Pb zircon and monazite geochronology of high-pressure pelitic granulites in the Jiaobei massif of the North China Craton. *Am. J. Sci.* **2008**, *308*, 328–350. [CrossRef]
27. Li, Z.; Chen, B. Geochronology and geochemistry of the Paleoproterozoic meta-basalts from the Jiao-Liao-Ji Belt, North China Craton: Implications for petrogenesis and tectonic setting. *Precambrian Res.* **2014**, *255*, 653–667. [CrossRef]
28. Liu, F.L.; Liu, C.H.; Itano, K.; Iizuka, T.; Cai, J.; Wang, F. Geochemistry, U-Pb dating, and Lu-Hf isotopes of zircon and monazite of porphyritic granites within the Jiao-Liao-Ji orogenic belt: Implications for petrogenesis and tectonic setting. *Precambrian Res.* **2017**, *300*, 78–106. [CrossRef]
29. Liu, P.H.; Liu, F.L.; Tian, Z.H.; Cai, J.; Ji, L.; Wang, F. Petrological and geochronological evidence for Paleoproterozoic granulite-facies metamorphism of the South Liaohe Group in the Jiao-Liao-Ji Belt, North China Craton. *Precambrian Res.* **2019**, *327*, 121–143. [CrossRef]
30. Wang, F.; Liu, F.L.; Liu, P.H.; Cai, J.; Schertl, H.P.; Ji, L.; Liu, L.S.; Tian, Z.H. In situ zircon U-Pb dating and whole rock geochemistry of metasedimentary rocks from South Liaohe Group, Jiao-Liao-Ji orogenic belt: Constraints on the depositional and metamorphic ages, and implications for tectonic setting. *Precambrian Res.* **2017**, *303*, 764–780. [CrossRef]
31. Cheng, C.Q.; Zhang, J.; Liu, J.; Zhao, C.; Yin, C.Q.; Qian, J.H.; Gao, P.; Liu, X.G.; Chen, Y. Geochemistry and petrogenesis of ca. 2.1 Ga meta-mafic rocks in the central Jiao–Liao–Ji Belt, North China Craton: A consequence of intracontinental rifting or subduction? *Precambrian Res.* **2022**, *370*, 106553. [CrossRef]
32. Liu, C.H.; Liu, F.L.; Zhao, G.C.; Tian, Z.H.; Cai, J.; Zhu, J.J.; Sun, X. Using multiple methods to better constrain the depositional age of a meta-sedimentary succession: An example of the Laoling Group from the northeastern North China Craton. *Precambrian Res.* **2023**, *392*, 107058. [CrossRef]
33. Meng, E.; Liu, F.L.; Liu, P.H.; Liu, C.H.; Yang, H.; Wang, F.; Shi, J.R.; Cai, J. Petrogenesis and tectonic significance of Paleoproterozoic meta-mafic rocks from central Liaodong Peninsula, northeast China: Evidence from zircon U-Pb dating and in situ Lu–Hf isotopes, and whole-rock geochemistry. *Precambrian Res.* **2014**, *247*, 92–109. [CrossRef]
34. Bai, J. *The Precambrian Geology and Pb-Zn Mineralization in the Northern Margin of North China Platform*; Geological Publishing House: Beijing, China, 1993.
35. Wang, H.C.; Ren, Y.W.; Lu, S.N.; Kang, J.L.; Chu, H.; Yu, H.B.; Zhang, C.J. Stratigraphic units and tectonic setting of the Paleoproterozoic Liao-Ji orogen. *Acta Geosci. Sin.* **2015**, *36*, 583–598. (In Chinese with English Abstract)
36. Yuan, L.L.; Zhang, X.H.; Xue, F.H.; Han, C.M.; Chen, H.H.; Zhai, M.G. Two episodes of Paleoproterozoic mafic intrusions from Liaoning province, North China Craton: Petrogenesis and tectonic implications. *Precambrian Res.* **2015**, *264*, 119–139. [CrossRef]

37. Meng, E.; Wang, C.Y.; Li, Y.G.; Li, Z.; Yang, H.; Cai, J.; Ji, L.; Jin, M.Q. Zircon U-Pb-Hf isotopic and whole-rock geochemical studies of Paleoproterozoic metasedimentary rocks in the northern segment of the Jiao-Liao-Ji Belt, China: Implications for provenance and regional tectonic evolution. *Precambrian Res.* **2017**, *298*, 472–489. [CrossRef]
38. Xu, W.; Liu, F.L.; Tian, Z.H.; Liu, L.S.; Ji, L.; Dong, Y.S. Source and petrogenesis of Paleoproterozoic meta-mafic rocks intruding into the North Liaohe Group: Implications for back-arc extension prior to the formation of the Jiao-Liao-Ji Belt, North China Craton. *Precambrian Res.* **2018**, *307*, 66–81. [CrossRef]
39. Li, Z.; Chen, B.; Yan, X.L. The Liaohe Group: An insight into the Paleoproterozoic tectonic evolution of the Jiao-Liao-Ji Belt, North China Craton. *Precambrian Res.* **2019**, *326*, 174–195. [CrossRef]
40. Zhang, Q.S.; Yang, Z.S. *Early Crust and Mineral Deposits of Liaodong Peninsula*; Geological Publishing House: Beijing, China, 1988.
41. Luo, Y.; Sun, M.; Zhao, G.C.; Li, S.Z.; Ayers, J.C.; Xia, X.P.; Zhang, J.H. A comparison of U-Pb and Hf isotopic compositions of detrital zircons from the North and South Liaohe Groups: Constraints on the evolution of the Jiao-Liao-Ji Belt, North China Craton. *Precambrian Res.* **2008**, *163*, 279–306. [CrossRef]
42. Li, S.Z.; Zhao, G.C.; Sun, M.; Han, Z.Z.; Zhao, G.T.; Hao, D.F. Are the South and North Liaohe Groups different exotic terranes? Nd isotope constraints. *Gondwana Res.* **2006**, *9*, 198–208. [CrossRef]
43. Lan, T.G.; Fan, H.R.; Yang, K.F.; Cai, Y.C.; Wen, B.J.; Zhang, W. Geochronology, mineralogy and geochemistry of alkali-feldspar granite and albite granite association from the Changyi area of Jiao-Liao-Ji Belt: Implications for Paleoproterozoic rifting of eastern North China Craton. *Precambrian Res.* **2015**, *266*, 86–107. [CrossRef]
44. Wang, X.P.; Peng, P.; Wang, C.; Yang, S.Y. Petrogenesis of the 2115 Ma Haicheng mafic sills from the eastern North China Craton: Implications for an intra-continental rifting. *Gondwana Res.* **2016**, *39*, 347–364. [CrossRef]
45. Wang, X.P.; Peng, P.; Wang, C.; Yang, S.Y.; Söderlund, U.; Su, X.D. Nature of three episodes of Paleoproterozoic magmatism (2180 Ma, 2115 Ma and 1890 Ma) in the Liaoji Belt, North China with implications for tectonic evolution. *Precambrian Res.* **2017**, *298*, 252–267. [CrossRef]
46. Xu, W.; Liu, F.L.; Santosh, M.; Liu, P.H.; Tian, Z.H.; Dong, Y.S. Constraints of mafic rocks on a Paleoproterozoic back-arc in the Jiao-Liao-Ji Belt, North China Craton. *J. Asian Earth Sci.* **2018**, *166*, 195–209. [CrossRef]
47. Liu, C.H.; Zhao, G.C.; Liu, F.L.; Cai, J. The southwestern extension of the JiaoLiao-Ji belt in the North China Craton: Geochronological and geochemical evidence from the Wuhe Group in the Bengbu area. *Lithos* **2018**, *304–307*, 258–279. [CrossRef]
48. Liu, D.Y.; Wilde, S.A.; Wan, Y.S.; Wu, J.S.; Zhou, H.Y.; Dong, C.Y.; Yin, X.Y. New U-Pb and Hf isotopic data confirm Anshan as the oldest preserved segment of the North China Craton. *Am. J. Sci.* **2008**, *308*, 200–231. [CrossRef]
49. Liu, J.; Liu, Z.H.; Zhao, C.; Wang, C.J.; Peng, Y.B.; Zhang, H. Petrogenesis and zircon LA-ICP-MS U-Pb dating of newly discovered Mesoarchean gneisses on the northern margin of the North China Craton. *Int. Geol. Rev.* **2017**, *59*, 1575–1589. [CrossRef]
50. Wan, Y.S.; Ma, M.Z.; Dong, C.Y.; Xie, H.Q.; Xie, S.W.; Ren, P.; Liu, D.Y. Widespread late Neoarchean reworking of Meso- to Paleoarchean continental crust in the Anshan-Benxi area, North China Craton, as documented by U-Pb-Nd-Hf-O isotopes. *Am. J. Sci.* **2015**, *315*, 620–670. [CrossRef]
51. Wang, W.; Liu, S.W.; Santosh, M.; Wang, G.H.; Bai, X.; Guo, R.R. Neoarchean intra-oceanic arc system in the Western Liaoning Province: Implications for the Early Precambrian crust-mantle geodynamic evolution of the Eastern Block of the North China Craton. *Earth-Sci. Rev.* **2015**, *150*, 329–364. [CrossRef]
52. Wang, W.; Liu, S.W.; Cawood, P.A.; Bai, X.; Guo, R.R.; Guo, B.R.; Wang, K. Late Neoarchean subduction-related crustal growth in the Northern Liaoning region of the North China Craton: Evidence from ~2.55 to 2.50 Ga granitoid gneisses. *Precambrian Res.* **2016**, *281*, 200–223. [CrossRef]
53. Wang, W.; Cawood, P.A.; Liu, S.W.; Guo, R.R.; Bai, X.; Wang, K. Cyclic formation and stabilization of Archean lithosphere by accretionary orogenesis: Constraints from TTG and potassic granitoids, North China Craton. *Tectonics* **2017**, *36*, 1724–1742. [CrossRef]
54. Li, Z.S.; Shan, X.L.; Liu, J.; Zhang, J.; Liu, Z.H.; Cheng, C.Q.; Wang, Z.G.; Zhao, C.; Yu, H.C. Late Neoarchean TTG and monzogranite in the northeastern North China Craton: Implications for partial melting of a thickened lower crust. *Gondwana Res.* **2023**, *115*, 201–223. [CrossRef]
55. Zhao, G.C.; Cao, L.; Wilde, S.A.; Sun, M.; Choe, W.J.; Li, S.Z. Implications based on the first SHRIMP U-Pb zircon dating on Precambrian granitoid rocks in North Korea. *Earth Planet. Sci. Lett.* **2006**, *251*, 365–379. [CrossRef]
56. Zhao, L.; Zhai, M.G.; Nutman, A.P.; Oh, C.W.; Bennett, V.C.; Zhang, Y.B. Archean basement components and metamorphic overprints of the Rangnim Massif in the northern part of the Korean Peninsula and tectonic implications for the Sino-Korean Craton. *Precambrian Res.* **2020**, *344*, 105735. [CrossRef]
57. Wang, M.J.; Liu, S.W.; Fu, J.H.; Wang, K.; Guo, R.R.; Guo, B.R. Neoarchean DTTG gneisses in southern Liaoning Province and their constraints on crustal growth and the nature of the Liao-Ji Belt in the Eastern Block. *Precambrian Res.* **2017**, *303*, 183–207. [CrossRef]
58. Zhai, M.G.; Zhang, X.H.; Zhang, Y.B.; Wu, F.Y.; Peng, P.; Li, Q.L.; Li, Z.; Guo, J.H.; Li, T.S.; Zhao, L.; et al. The geology of North Korea: An overview. *Earth-Sci. Rev.* **2019**, *194*, 57–96. [CrossRef]
59. Yu, H.; Liu, J.; He, Z.; Liu, Z.; Cheng, C.; Hao, Y.; Zhao, C.; Zhang, H.; Dong, Y. Geochronology and Zircon Hf Isotope of the Paleoproterozoic Gaixian Formation in the Southeastern Liaodong Peninsula: Implication for the Tectonic Evolution of the Jiao-Liao-Ji Belt. *Minerals* **2022**, *12*, 792. [CrossRef]

60. Bi, J.H.; Ge, W.C.; Xing, D.H.; Yang, H.; Dong, Y.; Tian, D.X.; Chen, H.J. Palaeoproterozoic meta-rhyolite and meta-dacite of the Liaohe Group, Jiao-Liao-Ji Belt, North China Craton: Petrogenesis and implications for tectonic setting. *Precambrian Res.* **2018**, *314*, 306–324. [CrossRef]
61. Zhu, K.; Liu, Z.H.; Xu, Z.Y.; Wang, X.A.; Cui, W.L.; Hao, Y.J. Petrogenesis and tectonic implications of two types of Liaoji granitoid in the Jiao–Liao–Ji Belt, North China Craton. *Precambrian Res.* **2019**, *331*, 105369. [CrossRef]
62. Cai, J.; Liu, F.L.; Liu, P.H.; Wang, F.; Meng, E.; Wang, W.; Yang, H.; Ji, L.; Liu, L.S. Discovery of granulite-facies metamorphic rocks in the Ji'an area, northeastern Jiao–Liao–Ji Belt, North China Craton: Metamorphic P-T evolution and geological implications. *Precambrian Res.* **2017**, *303*, 626–640. [CrossRef]
63. Cai, J.; Liu, F.L.; Liu, C.H. A unique Paleoproterozoic HP–UHT metamorphic event recorded by the Bengbu mafic granulites in the southwestern Jiao–Liao–Ji Belt, North China. Craton. *Gondwana Res.* **2020**, *80*, 244–274. [CrossRef]
64. Zhang, S.H.; Zhao, Y.; Davis, G.A.; Ye, H.; Wu, F. Temporal and spatial variations of Mesozoic magmatism and deformation in the North China Craton: Implications for lithospheric thinning and decratonization. *Earth-Sci. Rev.* **2014**, *162*, 387–432. [CrossRef]
65. Liu, Y.S.; Gao, S.; Hu, Z.C.; Gao, C.G.; Zong, K.Q.; Wang, D.B. Continental and oceanic crust recycling-induced melt-peridotite interactions in the Trans-North China Orogen: U-Pb dating, Hf isotopes and trace elements in zircons from mantle xenoliths. *J. Petrol.* **2010**, *51*, 537–571. [CrossRef]
66. Ludwig, K.R. *ISOPLOT 3.00: A Geochronological Toolkit for Microsoft Excel*; Berkeley Geochronology Center: Berkeley, CA, USA, 2003.
67. Wu, F.Y.; Yang, Y.H.; Xie, L.W.; Yang, J.H.; Xu, P. Hf isotopic compositions of the standard zircons and baddeleyites used in U-Pb geochronology. *Chem. Geol.* **2006**, *234*, 105–126. [CrossRef]
68. Dong, Y.; Bi, J.H.; Xing, D.H.; Ge, W.C.; Yang, H.; Hao, Y.J.; Ji, Z.; Jing, Y. Geochronology and geochemistry of Liaohe Group and Liaoji granitoid in the Jiao-Liao-Ji Belt, North China Craton: Implications for petrogenesis and tectonic evolution. *Precambrian Res.* **2019**, *332*, 105399. [CrossRef]
69. Chen, J.S.; Xing, D.H.; Liu, M.; Li, B.; Yang, H.; Tian, D.X.; Yang, F.; Wang, Y. Zircon U-Pb chronology and geological significance of felsic volcanic rocks in the Liaohe Group from the Liaoyang area, Liaoning Province. *Acta Petrol. Sin.* **2017**, *33*, 2792–2810. (In Chinese with English Abstract)
70. Tarney, J. Geochemistry of Archaean high grade gneisses with implications as to the origin and evolution of the Precambrian curst. In *The Early History of the Earth*; Windley, B.F., Ed.; John Wiley: Hoboken, NJ, USA, 1976.
71. Winchester, J.A.; Park, R.G.; Holland, J.G. The geochemistry of Lewisian semipelitic schists from the Gairloch District, Wester Ross. *Scott. J. Geol.* **1980**, *16*, 165–179. [CrossRef]
72. Middlemost, E.A.K. Naming materials in the magma/igneous rock system. *Earth-Sci. Rev.* **1994**, *37*, 215–224. [CrossRef]
73. Winchester, J.A.; Floyd, P.A. Geochemical magma type discrimination: Application to altered and metamorphosed basic igneous rocks. *Earth Planet. Sci. Lett.* **1977**, *28*, 459–469. [CrossRef]
74. Sun, S.S.; McDonough, W.F. Chemical and isotopic systematics of oceanic basalts: Implications for mantle composition and processes. *Geol. Soc. Lond. Spec. Publ.* **1989**, *42*, 313–345. [CrossRef]
75. Wang, M.J.; Liu, S.W.; Wang, W.; Wang, K.; Yan, M.; Guo, B.R.; Bai, X.; Guo, R.R. Petrogenesis and tectonic implications of the Neoarchean North Liaoning tonalitic-trondhjemitic gneisses of the North China Craton, North China. *J. Asian Earth Sci.* **2016**, *131*, 12–39. [CrossRef]
76. Cheng, C.Q.; Liu, J.; Zhang, J.; Chen, Y.; Yin, C.Q.; Liu, X.G.; Qian, J.H.; Gao, P.; Wang, X. Petrogenesis of newly identified Neoarchean granitoids in the Qingyuan of NE China: Implications on crustal growth and reworking of the North China Craton. *J. Asian Earth Sci.* **2022**, *236*, 105333. [CrossRef]
77. Sun, M.; Armstrong, R.L.; Lambert, R.S.; Jiang, C.C.; Wu, J.H. Petrochemistry and Sr, Pb and Nd isotopic geochemistry of Paleoproterozoic Kuandian Complex, the eastern Liaoning Province, China. *Precambrian Res.* **1993**, *62*, 171–190.
78. Peng, Q.M.; Palmer, M.R. The Paleoproterozoic boron deposits in eastern Liaoning, China: A metamorphosed evaporate. *Precambrian Res.* **1995**, *72*, 185–197. [CrossRef]
79. Liu, J.H.; Wang, X.J.; Chen, H. Intracontinental extension and geodynamic evolution of the Paleoproterozoic Jiao-Liao-Ji Belt, North China Craton: Insights from coeval A-type granitic and mafic magmatism in eastern Liaoning Province. *Geol. Soc. Am. Bull.* **2021**, *133*, 1765–1792. [CrossRef]
80. Li, S.Z.; Zhao, G.C. SHRIMP U-Pb zircon geochronology of the Liaoji granitoids: Constraints on the evolution of the Paleoproterozoic Jiao-Liao-Ji belt in the Eastern Block of the North China Craton. *Precambrian Res.* **2007**, *158*, 1–16. [CrossRef]
81. Wan, Y.S.; Song, B.; Liu, D.Y.; Wilde, S.A.; Wu, J.S.; Shi, Y.R.; Yin, X.Y.; Zhou, H.Y. SHRIMP U-Pb zircon geochronology of Paleoproterozoic metasedimentary rocks in the North China Craton: Evidence for a major Late Paleoproterozoic tectonothermal event. *Precambrian Res.* **2006**, *149*, 249–271. [CrossRef]
82. Zhang, Y.F.; Liu, J.D.; Xiao, R.G.; Wang, S.Z.; Wang, J.; Bao, D.J. The Hyalotourmalites of Houxianyu Borate Deposit in Eastern Liaoning: Zircon Features and SHRIMP Dating. Earth Sci. *J. China Univ. Geosci.* **2010**, *35*, 985–999. (In Chinese with English Abstract)
83. Li, Z.; Chen, B.; Liu, J.W.; Zhang, L.; Yang, C. Zircon U-Pb ages and their implications for the South Liaohe Group in the Liaodong Peninsula, Northeast China. *Acta Petrol. Sin.* **2015**, *31*, 1589–1605. (In Chinese with English Abstract)
84. Chen, B.; Li, Z.; Wang, J.; Zhang, L.; Yan, X. Liaodong peninsula ~2.2 Ga magmatic event and its geological significance. *J. Jilin Univ.* **2016**, *46*, 303–320. (In Chinese with English Abstract)

85. Lu, X.; Wu, F.; Lin, J.; Sun, D.; Zhang, Y.; Guo, C. Geochronological successions of the early Precambrian granitic magmatism in southern Liaodong Peninsula and its constraints on tectonic evolution of the north China craton. *Chin. J. Geol.* **2004**, *39*, 123–138. (In Chinese with English Abstract)
86. Yang, M.C.; Chen, B.; Yan, C. Petrogenesis of Paleoproterozoic gneissic granites from Jiao-Liao-Ji Belt of North China Craton and their tectonic implications. *J. Earth Sci. Environ.* **2015**, *37*, 31–51. (In Chinese with English Abstract)
87. Song, Y.H.; Yang, F.C.; Yan, G.L.; Wei, M.H.; Shi, S.S. SHRIMP U-Pb age and Hf isotopic compositions of Paleoproterozoic granites from the eastern part of Liaoning Province and their tectonic significance. *Acta Geol. Sin.* **2016**, *90*, 2620–2636. (In Chinese with English Abstract)
88. Wang, P.S.; Dong, Y.S.; Li, F.Q.; Gao, B.S.; Gan, Y.C.; Chen, M.S.; Xu, W. Paleoproterozoic granitic magmatism and geological significance in Huanghuadian area, eastern Liaoning Province. *Acta Petrol. Sin.* **2017**, *33*, 2708–2724. (In Chinese with English Abstract)
89. Wang, X.J.; Liu, J.H.; Ji, L. Zircon U-Pb chronology, geochemistry and their petrogenesis of Paleoproterozoic monzogranitic gneisses in Kuandian area, eastern Liaoning Province, Jiao-Liao-Ji Belt, North China Craton. *Acta Petrol. Sin.* **2017**, *33*, 2689–2707. (In Chinese with English Abstract)
90. Zhou, Y.Y.; Sun, Q.Y.; Zhao, T.P.; Zhai, M.G. Petrogenesis of the early Paleoproterozoic low-δ^{18}O potassic granites in the southern NCC and its possible implications for no confluence of glaciations and magmatic shutdown at ca. 2.3 Ga. *Precambrian Res.* **2021**, *361*, 106258. [CrossRef]
91. Yang, J.H.; Chung, S.L.; Wilde, S.A.; Wu, F.Y.; Chu, M.F.; Lo, C.H.; Fan, H.R. Petrogenesis of post-orogenic syenites in the Sulu Orogenic Belt, East China: Geochronological, geochemical and Nd–Sr isotopic evidence. *Chem. Geol.* **2005**, *214*, 99–125. [CrossRef]
92. Foland, K.A.; Allen, J.C. Magma sources for Mesozoic anorogenic granites of the White Mountain magma series, New England, USA. *Contrib. Miner. Petrol.* **1991**, *109*, 195–211. [CrossRef]
93. Turner, S.P.; Foden, J.D.; Morrison, R.S. Derivation of some A-type magmas by fractionation of basaltic magma; an example from the Padthaway Ridge, South Australia. *Lithos* **1992**, *28*, 151–179. [CrossRef]
94. Sisson, T.W.; Ratajeski, K.; Hankins, W.B.; Glazner, A.F. Voluminous granitic magmas from common basaltic sources. *Contrib. Miner. Petrol.* **2005**, *148*, 635–661. [CrossRef]
95. Eliwa, H.A.; El-Bialy, M.Z.; Murata, M. Ediacaran post-collisional volcanism in the Arabian-Nubian Shield: The high-K calc-alkaline Dokhan Volcanics of Gabal Samr El-Qaa (592 ± 5 Ma), North Eastern Desert, Egypt. *Precambrian Res.* **2014**, *246*, 180–207. [CrossRef]
96. Beard, J.S.; Lofgren, G.E. Dehydration melting and water-saturated melting of basaltic and andesitic greenstones and amphibolites at 1, 3, and 6.9 kb. *J. Petrol.* **1991**, *32*, 365–401. [CrossRef]
97. Nakajima, K.; Arima, M. Melting experiments on hyrous low-K tholeiite: Implications for the genesis of tonalitic crust in the Izu-Bonin-Mariana arc. *Isl. Arc* **1998**, *7*, 359–373. [CrossRef]
98. Frost, C.D.; Frost, B.R.; Chamberlain, K.R.; Edwards, B. Petrogenesis of the 1.43 Ga Sherman batholith, SE, Wyoming, USA: A reduced, rapakivi-type anorogenic granite. *J. Petrol.* **1999**, *40*, 1771–1802. [CrossRef]
99. Maurice, A.E.; Gharib, M.E.; Wilde, S.A.; Ali, K.A.; Osman, M.S.M. Subduction to post-collisional volcanism in the Northern Arabian-Nubian Shield: Genesis of Cryogenian/Ediacaran intermediate-felsic magmas and the lifespan of a Neoproterozoic mature island arc. *Precambrian Res.* **2021**, *358*, 106148. [CrossRef]